FEATURE BASED ADAPTIVE MOTION MODEL FOR BETTER LOCALIZATION

by

Rohan Bhargava

Submitted in partial fulfillment of the
requirements for the degree of
Master of Computer Science

at

Dalhousie University
Halifax, Nova Scotia
October 2014

DALHOUSIE UNIVERSITY

FACULTY OF COMPUTER SCIENCE

The undersigned hereby certify that they have read and recommend to the Faculty of Graduate Studies for acceptance a thesis entitled "FEATURE BASED ADAPTIVE MOTION MODEL FOR BETTER LOCALIZATION" by Rohan Bhargava in partial fulfillment of the requirements for the degree of Master of Computer Science.

Dated: October 1, 2014

Supervisors:

Dr. Thomas Trappenberg

Dr. Mae Sato

Readers:

Dr. Evangelos E. Milios

A. External

DALHOUSIE UNIVERSITY

DATE: October 1, 2014

AUTHOR: Rohan Bhargava

TITLE: FEATURE BASED ADAPTIVE MOTION MODEL FOR BETTER LOCALIZATION

DEPARTMENT OR SCHOOL: Faculty of Computer Science

DEGREE: M.C.Sc. CONVOCATION: May YEAR: 2014

Signature of Author

Table of Contents

List of Tables

List of Figures

Abstract

Acknowledgements

I would like to thank my colleagues at Hallab for their encouragement and support throughout my work. I would like to express my special appreciation and thanks to my supervisors Dr. Thomas Trappenberg and Dr. Mae Sato. I would like to thank them for encouraging my research and for allowing me to grow as a research scientist. A special thanks to my family for all the sacrifices they have made for me to pursue my research interests. Last but certainly the least my deepest gratitude goes to my late grandfather, Dr. D.N. Bhargava. His words of wisdom and encouragement from above has a great impact on what I am and I dedicate my thesis to him. Thankyou

Chapter 1

Introduction

1.1 Motivation

The core of human environment interaction is the ability of a person to know its position in surrounding environment. The process of estimating the robot's position and orientation in the world is termed as Localization [33]. A common approach to determine the location of a robot is through the use of a Global Positioning System (GPS) which uses a series of satellites in low earth orbit that use differential positioning to determine a location for a receiver. Another approach is to provide a prior map of the environment and with the help of sensors a robot perceives the world and localizes itself in it. The major challenge to localization is sensing external environment can be impossible or incomplete due to unreliability and inaccessibility of the sensors. In this case the localization estimate can be updated using self-generated cues such as acceleration and velocity.

An example for such a scenario from underwater robotics is maintaining a pose estimate of an Autonomous Underwater Vehicle(AUV). In AUV the pose estimation relies on Inertial Navigation Systems (INS) which gives an estimate of the velocity, position and orientation. An example of such a vehicle is Hugin 4500 (Figure 1.1). All INS systems suffer from drift i.e. small errors in measurement of acceleration and angular velocity are integrated into progressively larger error. To compensate for drift systems such as Doppler Velocity Log (DVL), surface GPS etc. are used [18] [20]. Hegrenaes et al [14] pointed out that there are situations where these systems fail or readings from these sensors need to be discarded due to poor quality. An example of such a situation is the non-feasibility of the vehicle to surface. In such situations they proposed to use the self-generated velocity estimates to aid INS systems.

The estimates can be difficult to acquire and maintain due to uncertainties in way a robot interacts and senses its environment. These uncertainties can arise due to noisy and incomplete sensing of the environment, uncertain movements of a robot

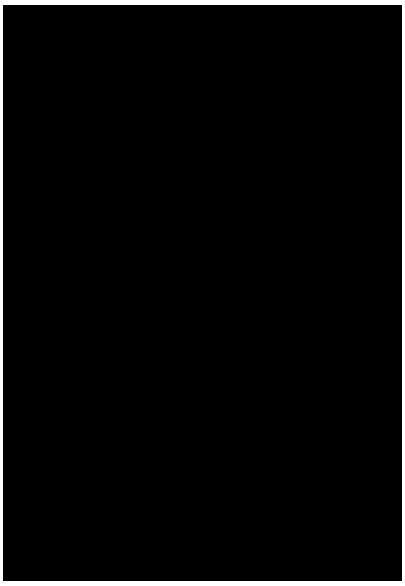

Figure 1.1: Hugin 4500 autonomous underwater vehicles. When submerged, the vehicle uses dead reckoning, incorporating DVL and compass input to maintain an estimate on current positioning.

in the environment and changes in the environment itself. To address these issues Sebastian Thrun [33] represented the motion and sensor models probabilistically. This helps in having a probability distribution over a space of guesses instead of relying on a single best guess. To update the state of a robot probabilistically there are algorithms such as Kalman Filter [16], Particle Filter [11] etc. which are based on Bayes filter.

In probabilistic robotics the motion and sensors models are represented by a distribution which is defined by its parameters. The process of determining parameters to kinematic model is termed calibration [4] [37]. Generally the parameters to the models are hand tuned and are derived by conducting calibration experiments. Such calibration methods are impractical for two reasons. Firstly these processes are labour intensive and require prior information about the environment and robot. Secondly, changes in robot (e.g.-: general wear and tear) and environment (e.g.-: moving from fresh water to sea water) leads to changes in the parameters. The changes in underwater environments can be due to change in density, temperature etc. of water. These changes require recalibration of a robot while it is in operation which in most cases is not possible to do. The inaccuracies in the models will effect results for higher level

tasks such as path planning [19], Simultaneous Localization and Mapping (SLAM) [33] [12] etc.

1.2 Previous Work

Home News by technology Ubuntu derivatives: 5 of the best Ubuntu-based distros Ubuntu derivatives: 5 of the best Ubuntu-based distros ROUNDUP Our pick of the best Ubuntu re-spins By Mayank Sharma from Linux Format Issue 173 August 4th 2013 4 COMMENTS

The best re-spins for Ubuntu for those who don't like Unity Related stories Expect an influx of Ubuntu phones in 2014 CompuLab readies MintBox 2 with fresh internals 50 best Linux distros: find the best one for you Are you a Linux desktop user who loves Ubuntu but is wary of Unity? You're in luck. There are lots of Ubuntu spins, both from Canonical and independent developers, which preserve the basic infrastructure and essence of Ubuntu but replace the default Unity desktop. Canonical has been producing official spins since its second release, but they have been getting more attention since Ubuntu switched to Unity. The oldest, and one of the most popular, is Kubuntu, which offers the KDE desktop; if you want Ubuntu goodness on an underpowered computer, there's the lightweight Lubuntu; and starting with the 13.04 Raring Ringtail release, users will also be able to use the Gnome desktop thanks to the new Ubuntu Gnome spin. As well as these official spins, many independent developers use Ubuntu as the base for their own distros. While most of these are just the stock Ubuntu release with a few added applications, some developers put in the extra effort. You might also like...

8 of the best tiny Linux distros How to dual-boot Linux and Windows 24 things we'd change about Linux Beginner's guide to Linux Bodhi Linux is a semi-rolling distro that's based on the stable Ubuntu Long Term Support (LTS) releases. It installs an elegant-looking, minimal system that can be customised easily to suit a regular desktop or a dated machine. Also featured is Zorin OS, designed to appease users moving from Windows. How we tested...

Comparing the distros was tricky. As they're all underpinned by Ubuntu, the usual parameters for comparison, such as installation, were very similar. The main

reason for this roundup is to help you select a distro that gives you a better desktop experience than Unity. Another important point of comparison is system requirements. Unity requires accelerated graphics, which makes the standard Ubuntu unsuitable for older computers. We also paid attention to the custom tools shipped with some distros that have their own package manager. Some replace the default tools with their particular desktop environment to increase usability. No distro comparison is complete without a look at bundled apps and configuration options, and even more so, since both of these factors depend on the desktop environment. Default apps

For most distros in this roundup, the choice of default software depends on the desktop. So you'll find Gnome-apps such as Evolution, Shotwell, Rhythmbox and Totem in Ubuntu Gnome, and KDE-apps such as Kmail, Amarok and Dragon Player in Kubuntu. Although both of these distros try to remain true to their desktops, there are some exceptions. Most notable is LibreOffice, the default suite in Ubuntu Gnome, Kubuntu and Zorin. The lightweight Lubuntu uses AbiWord and Gnumeric instead, and Bodhi ships with only a basic text editor. In fact, the only real app in Bodhi is the Midori web browser, which you can use to access Bodhi's online app store and download new apps. Interestingly, Google Docs thinks of Midori as an outdated version of Google Chrome. Zorin ships with the real proprietary Google Chrome, while Lubuntu includes its open source sister, Chromium. Instead of Gnome's Epiphany browser (now rechristened simply Web), Ubuntu Gnome includes Firefox. Kubuntu ships with its own Reconq browser, although it does have a shortcut to install Firefox. In stark contrast to Bodhi, the other lightweight distro, Lubuntu is chock full of apps. It's got some GTK apps such as the document viewer Evince, Archive Manager and image editor mtPaint, along with feature-weight apps that go with its LXDE desktop, such as the Leafpad text editor and PCManFM. Lubuntu also has the Sylpheed email client and the Chromium web browser. It's also got Audacious and Gnome Mplayer so you can play most popular formats: MP3s, AVIs and MP4s etc. Ubuntu Gnome also lets you play MP3s out of the box with Rhythmbox. You won't find any plugins under Kubuntu but its multimedia apps are designed to fetch codecs as and when they are needed. The best thing about the Ubuntu derivatives is that you can install proprietary plugins and codecs to play restricted formats while installing the distro. Zorin is the only distro in this roundup that lets you view content in

proprietary formats from within the live environment. At 1.5GB, Zorin is the heaviest distro. Besides the apps already mentioned, it includes Gimp, Shotwell, Google Chrome, Gwibber, Thunderbird, Empathy, Totem, Rhythmbox, VLC and even the OpenShot video editor. It also includes Wine to install Windows-only apps. Unless you are using Zorin, you'll need to pay a visit to the distro's package management app soon after installing. In Bodhi, it's the first thing you'll need to do, while Lubuntu, Ubuntu Gnome and Kubuntu can give you a fair amount of mileage with their default selection. Verdict Ubuntu Gnome - 3/5 Kubuntu - 3/5 Lubuntu - 4/5 Bodhi Linux - 1/5 Zorin - 5/5 Intended purpose

The distros we've chosen provide a different GUI to Unity, but they each ensure the distro works well for its intended audience. The aim of the Ubuntu Gnome spin is to provide a relatively pure Gnome desktop. Since the main Ubuntu distro still uses libraries from Gnome 3.6, Ubuntu Gnome 13.04 ships with an older Gnome release, and users will have to manually install the latest Gnome from the Person Package Archive (PPA). Users will also miss out on new Gnome apps, such as Boxes and Web, which depend on libraries from the latest release. Kubuntu does for KDE what Ubuntu Gnome does for Gnome Shell. But Kubuntu nicely integrates the KDE desktop. That said, it doesn't include all apps developed by the KDE project, most notably the Calligra Office Suite. The Lubuntu developers wanted to create a less resource-hungry distro and LXDE fits the bill. Lubuntu also includes software like Mplayer, which makes it more usable than its peers. Bodhi Linux is also a lightweight distro, but encourage users to customise the system, handled nicely by its package management system. Lastly, Zorin OS is designed for Windows users, and pulls this off brilliantly thanks to its default interface and the custom Look Changer app. Verdict Ubuntu Gnome - 2/5 Kubuntu - 4/5 Lubuntu - 5/5 Bodhi Linux - 5/5 Zorin - 5/5 Desktop Experience

Before Unity, Ubuntu was the most popular Linux distro for desktop users - and for good reason. It has the best-in-class Ubiquity distro installer, as well as an easy-to-use package management system that allows users to upgrade with a single click. All distros in this roundup share the same lineage. While some need more resources to run comfortably, what sets them apart from Ubuntu and each other is how they look, and how you operate them. This is also the main reason why you would want

to use an Ubuntu derivative instead of the real thing. The questions were asking are: do the spins appeal to new Linux users coming in from other OSes, such as Windows and Mac OS? And if you're an existing Linux user, who had Ubuntu in the past, which spin returns to the pre-Unity days? Ubuntu Gnome - 2/5

If you were disappointed by Unity, then the desktop environment Ubuntu Gnome offers is unlikely to make you happy either. There are a number of similarities between Gnome 3 and Unity, although they each go about implementing them differently. If you dislike Unity's vertical launcher, you probably won't be that keen on the similar launcher in Gnome. And while the launcher in Unity is always visible, in Gnome you have to bring up the Activities View before you can even see it. Gnome's other low points are minimal window furniture and the inability to create desktop icons, which make it a distro that's only likely to please existing Gnome users. In fact, even existing Gnome users won't like this spin, because it ships with the older Gnome 3.6. Kubuntu - 3/5

At first glance KDE looks very much like Windows: it's got a Taskbar-like panel at the bottom of the screen, a launch menu in the corner, quicklaunch icons, and a notification area with tray icons. But to pitch KDE to new users as simply 'looking like Windows' is doing the desktop environment a disservice. Its real power lies in the vast configuration options and features like Activities, which, sadly, users will find confusing or, at worst, totally ignore. Activities are, in fact, custom workspaces or virtual desktops that you can setup and switch between for a given activity, for example a desktop ready with all the apps open for some web development. Kubuntu is the oldest Ubuntu spin, it has an active community of users and it's the go-to distro for users burnt by Unity, but it's missing some of Ubuntu's best features, such as the Software Center. Lubuntu - 3/5

Like KDE, Lubuntu's LXDE desktop is similar to Windows, with a panel at the bottom. The menu, though, is reminiscent of Windows 98. When you think about it, a Windows 98 look-a-like won't really lure Windows 7/XP users, especially when you consider the fact that LXDE doesn't have other Windows features, such as live thumbnail previews. Additionally, Lubuntu lacks Ubuntu One, and integration with PCManFM and Sylpheed is still on the developers' to-do list. But then Lubuntu is aimed at a different set of users: those who want to run an Ubuntu-like desktop on an

old, underpowered machine. This is something Lubuntu does remarkably well. The fact it also supplies a pleasant desktop environment is an added bonus. Bodhi Linux - 2/5

Another minimalist distro, Bodhi Linux is based on the elegant Enlightenment Window Manager and has its own file manager, several gadgets and compositing effects. With Bodhi you can bring an old machine back to life in style. The distro also offers several different desktop layout styles: Desktop is a traditional layout with a menu, Taskbar and System Tray at the bottom; Laptop/Netbook puts the System Tray, menu and Taskbar on the top, along with some gadgets, and moves the application launcher to the bottom; while Fancy places the application launcher on the left of the screen. There's also a style for small/touchscreen devices, which uses an application menu like Unity's Dash or Gnome 3's Activities. Zorin OS - 5/5

This is hands-down the best distro, offering the ultimate desktop experience for existing Linux users, as well as those coming from other operating systems. Not only is the default Zorin desktop styled to resemble Windows 7, for added familiarity, its custom application launcher also mimics the Windows 7 Start menu. Existing Linux users can use the Zorin Look Changer app to make the desktop act and look like Gnome 2. If you can spare 10, you can download the Ultimate edition, which has additional Mac OS X and Windows 2000 styles. Zorin also includes all of the Ubuntu goodies, such as Ubuntu One, which is well integrated into the distro. It also instills good desktop practices by regularly reminding users to setup the backup app. System requirements

Due to the different system requirements of their desktop environments, some of the spins might not run on all kinds of hardware. The most demanding distro in our roundup is Ubuntu Gnome thanks to the desktop's insistence on using accelerated graphics. On the other hand, you can run KDE, and therefore Kubuntu, on a computer that doesn't have a discrete graphics card installed. The desktop will, instead, default to having only the most basic compositing effects, but it will remain fully functional. If you need a distro for an older box, neither Ubuntu Gnome nor Kubuntu will work as well as Lubuntu or Bodhi Linux. To productively use the LXDE-based Lubuntu you'll need at least 512MB of RAM. The project also produces special installation ISOs for computers with less than 700MB RAM. Bodhi Linux goes down

even further. You can install it on a system with 128MB of RAM and it only takes up 2.5GB of hard disk space. The good thing about Bodhi is that it can scale up just as easily on a more recent, well-endowed machine. Just use its package manager to fetch the application suite of full-featured software instead of the lighter-weight packages. Zorin OS gives you the best of both worlds. While the normal version is based on Gnome and requires the same amount of resources as Kubuntu, there's also a LXDE-based Lite edition for older computers. Verdict Ubuntu Gnome - 1/5 Kubuntu - 3/5 Lubuntu - 4/5 Bodhi Linux - 5/5 Zorin - 4/5 Documentation and support

One of the reasons Ubuntu is so popular is the support infrastructure and its active community of users. But how do the derivatives fair? Ubuntu Gnome has a growing community with its own IRC channel and a mailing list, and while it doesn't have forum boards it regularly dispenses help to users on its official Google+ Community page. The oldest Ubuntu spin, Kubuntu, has a very active community that hosts KDE-specific forums, mailing lists and an IRC channel. The distro also has information on getting help in languages other than English, and there's a comprehensive ebook guide available on ubuntuguide.org. Lubuntu hosts its documentation and support on Ubuntu infrastructure. There's documentation about the various applications and how to set up different components. The link to the forums shows all posts with the tag 'lubuntu' on ubuntuforums.org. You can interact with Lubuntu developers on its mailing lists and IRC. Zorin OS has a very rudimentary installation guide, though they have forum boards with a tutorial section. Shelling out 5 will get you premium technical support for three issues. Bodhi Linux has the most organised support and documentation. There's a quick start guide, and detailed guides on Enlightenment and customising Bodhi. It's forum boards even dispense advice on ARM-powered devices. Verdict Ubuntu Gnome - 2/5 Kubuntu - 3/5 Lubuntu - 2/5 Bodhi Linux - 5/5 Zorin - 2/5 Custom Tools

As we've already said, what sets our contenders apart from the myriad of Ubuntu-based distros is the developer effort that's gone into fitting the distro to its user base. Consider Zorin, for example. It's designed specifically for Windows users who want easy and smooth access to Linux, so it includes a custom Look Changer application that lets you change the interface at the touch of a button. In the freely downloadable

edition of the OS, the application offers a choice of Windows 7, XP or Gnome 2. Donate 10 for the Ultimate edition and you also get support for Mac OS X, Unity and Windows 2000. Zorin's Web Browser Manager makes it easy to install different browsers and the distro also includes a redesigned Ubuntu Software Center. Bodhi Linux is all about custom tools. It ships with the Eccess System Tool for basic system administration tasks, such as managing users and time. There's a board on the Bodhi Linux forum dedicated to custom apps written in Elementary and Python that are available in the official repositories. Another highlight is its online App Center, which makes installing apps easier by grouping them into software bundles and creating custom packages of similar tools. For example, if you want to install a selection of different educational apps, you can install the Educational Pack, which includes TuxPaint, TuxTyping, Gcompris etc. The developers of Lubuntu dealt with package management by creating a lightweight version of Ubuntu Software Center called - you guessed it! - Lubuntu Software Center. This arranges software in different categories, you mark apps that you want to install, add them to the apps basket and install them all in one go. The tool also has an Expert mode for installing individual libraries. Kubuntu also includes its own package manager, Moun, and the HomeRun launcher, which runs full screen and is similar to Unity's Dash and Gnome's Activities. The one spin that doesn't have any custom tools is Ubuntu Gnome. The distro includes the stock Ubuntu Software Center and is, in fact, missing some Gnome tools like the web browser and the Boxes virtualisation app. This is further confused by the fact that the distro includes two User Accounts apps, one from Gnome and from Ubuntu. Verdict Ubuntu Gnome - 1/5 Kubuntu - 2/5 Lubuntu - 3/5 Bodhi Linux - 5/5 Zorin - 5/5 Configuration options

Most distros delegate the task of customising the desktop to the GUI. This is quite a disadvantage for Ubuntu Gnome as its default customisation settings will work for the average user but the more advanced Linux user will need to get additional tools to tweak their desktops. On the other end of the spectrum is KDE and its endless configuration options, which can be overwhelming. Lubuntu also has lots of configuration options. There's an Openbox configuration manager and a customiser from the LXDE project. There are also different apps for modifying keyboard, mouse, monitor and power management etc. Kubuntu, in contrast, doesn't have its own set

of configuration tools like OpenSUSE's Yast or Mageia's Control Center.

Roy and Thrun [26] proposed an online calibration method for land robots which can be performed without human intervention. They approached the calibration process as maximum likelihood estimation problem which gives an estimate of parameters for the given data. The calibration parameters are iteratively estimated by comparing pair of subsequent sensor readings. The algorithm proposed worked well for systematic drifts and the results showed the position error reduced by approximately by 83%.

Alizar and Parr [8] continued the work further by estimating non-systematic drifts. They proposed an algorithm to learn the right parameters of a motion model for a land robot using Expectation Maximization Framework [5]. It is an unsupervised machine learning technique that alternates between the expectation and maximization step. In the Expectation Step it creates an expectation of the log-likelihood using the current estimate of the parameters and the Maximization step which computes parameters maximizing the expected log-likelihood found in the Expectation Step. They were able to learn accurate motion models with very little user input.

Yapp [38] took Alizar and Parr's [8] work further and proposed an algorithm to learn the motion and sensor models for land robots. They used the same Expectation Maximization framework to learn the right parameters for the models. To calculate the likely trajectory of a robot both the algorithms implemented particle filtering [24] [3] and smoothing [6]. The algorithm started with an estimate of initial parameters and iteratively optimized the parameters based on the data collected during robot's operation. The algorithm assumed that a prior map of the environment is provided.

1.3 Contribution

In my thesis I specifically deal with water environments such as oceans, rivers etc. which are highly dynamic. The algorithm proposed here is different from the work done before in two ways. Firstly the algorithm is meant to learn the right parameters for an AUV's motion model. Secondly, the algorithm can learn motion model for unknown environments by generating landmarks using side sonar images and therefore doesn't have to rely on static maps. Sound Navigation and Ranging (SONAR) is a technique based on sound propagation used for detecting objects underwater. Side

scan sonar is a specific type of sonar used to image the topography of a sea floor. The SONAR sensor is the only imaging tool that can work at high depth.

My algorithm uses EM algorithm to calculate the most likely parameters for a data set. The trajectories are calculated by implementing particle filtering and smoothing. Particle Filters are chosen because they can mode non-linear transformations as well as have no restrictions in model. Particle smoothing was performed because Russel and Norving [27] pointed out that the state of the system is better estimated by smoothing as it incorporates information from all the past states of the system.

The remainder of the thesis is structured as follows. Chapter 2 will explain the motion model for AUV as well as give an insight on particle filtering and smoothing. Chapter 3 will give an overview of Expectation Maximization and show how this framework is used to adapt parameters for a motion model. Chapter 4 will give explain how landmarks are extracted from side sonar images. The reliability of the landmarks are shown by extracting motion information and the algorithm to do that is described in Chapter 4. Chapter 5 consist results of a simulated experiment to show the effectiveness of the algorithm. This chapter also includes the comparison of motion estimation using side sonar images to Doppler velocity log (DVL).

Chapter 2

Background

In the chapter we start by discussing how motion models are probabilistically represented as well as give an insight about motion models for AUV. This helps us in understanding of how motion model captures the probabilistic movements of robots. We then discuss a probabilistic state estimation algorithm such as particle filter [24] [3] which is at the heart of my algorithm as well as many other robotics systems. Lastly we discuss about particle smoothing [6] [7] which gives an estimate of ground truth by calculating the distribution of past states with taking into account all the evidence up to present.

2.1 Motion Model

A motion model is responsible for capturing the relationship between the control input and the change in robot's configuration. Thrun [33] models the motion of a robot probabilistically because the same control inputs will never reproduce the same motion. A good motion model will capture the errors such as drift that are encountered during the motion of a robot. The motion model is a necessary ingredient of many algorithms such as localization,mapping etc.

Let $X = (x, y, \theta)$ be the initial pose of the robot in x-y space. Mathematically the motion model can be described as $P(X^{'}|X, u)$, where $X^{'}$ is the pose after executing the motion command u. Based on the control input Thrun [33] divided the motion model in two classes

1. Odometry based motion model -:
   The class of motion models are used for robots equipped with wheel encoders. Odometry is generally obtained by integrating wheel encoders information and is more accurate than velocity.

2. Velocity based motion model -:

These models calculate the new position based on velocities and time elapsed. These models are implemented for Autonomous Underwater Vehicle(AUV) and Unmanned Aerial Vehicles(UAV). Both odometry as well as velocity suffer from drift and slippage therefore the same control commands will not generally reproduce the same motion.

The velocity motion model proposed by Thrun [33] assumes that robot can be controlled through two velocities a rotational and translational velocity. The translational velocity at time t is denoted by v_t and rotational velocity by w_t. Hence the control input u_t can be represented by

$$u_t = \begin{pmatrix} v_t \\ w_t \end{pmatrix}$$

The assumption is that positive rotational velocities w_t induce a counterclockwise rotation whereas positive translational velocities v_t correspond to forward motion. The set of equations to compute the next state of a robot for a velocity motion model are

$$x_t = x_{t-1} + v_{t-1}/w_{t-1}\sin(\theta_{t-1}) + v_{t-1}/w_{t-1}\cos(\theta_{t-1} + w_{t-1}\delta t) \tag{2.1}$$

$$y_t = y_{t-1} + v_{t-1}/w_{t-1}\cos(\theta_{t-1}) - v_{t-1}/w_{t-1}\sin(\theta_{t-1} + w_{t-1}\delta t) \tag{2.2}$$

$$\theta_t = \theta_{t-1} + w_{t-1}\delta t \tag{2.3}$$

In an AUV a velocity motion model is implemented and to represent AUV's motion, 6 independent coordinates are necessary to determine the position and orientation of the rigid body. The notations used for marine vehicles are described in Table 2.1.

The pose of AUV can be represented as $s = (x, y, z, \theta, \phi, \psi)$. The first three coordinates correspond to the position along the x,y,z axes while the last three coordinates describe the orientation commonly termed as roll, pitch yaw. Fossen [32] in his book describes the motion of a marine vehicle in 6 DOF using two coordinate systems as shown in Figure 2.1. X_0, Y_0, Z_0 represent the moving coordinate frame and is called

DOF		forces and moments	linear and angular vel.	positions and Euler angles
1	motions in the x-direction (surge)	X	u	x
2	motions in the y-direction (sway)	Y	v	y
3	motions in the z-direction (heave)	Z	w	z
4	rotation about the x-axis (roll)	K	p	ϕ
5	rotation about the y-axis (pitch)	M	q	θ
6	rotation about the z-axis (heave)	N	r	ψ

Table 2.1: Notation used for marine vehicles. Table from [32]

as body-fixed reference frame. The earth-fixed reference frame is denoted by X, Y, Z. The origin of the body-reference frame is denoted by O and is chosen to coincide with the center of gravity denoted by CG.

To estimate the position of an AUV we need to calculate the velocity at which the AUV is currently moving. The velocity can be computed in two ways-: a) Static Motion model b) Dynamic Motion model

In the static model the velocity is calculated from a lookup table. In the dynamic model we are computing forces and moments on the fly but the parameters to these forces are considered to be static. The parameters such as density, temperature etc. of water can change with time and lead to an inaccurate estimate of velocity in both the models. Hence the velocity needs to be adapted and Chapter 3.2 explains how it is done in my algorithm. A detailed description on how the velocity is calculated in both the models is explained in rest of the chapter.

Hegrenaes [13] points that a way to implement a simple static motion model as table look-up based on experimental data.

$$u_r = f(n_s) \tag{2.4}$$

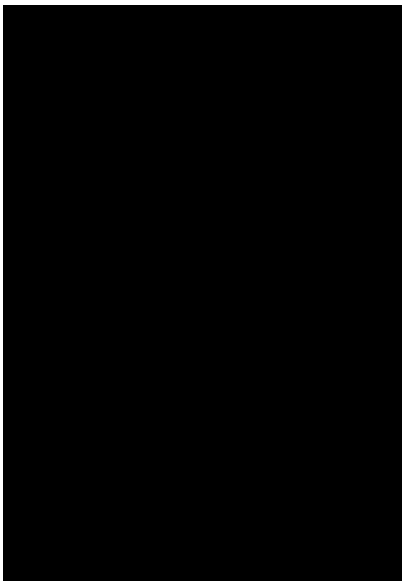

Figure 2.1: Body-fixed and earth-fixed reference frames to describe the coordinate system of an AUV. Figure from [32]

u_r, n_s are the water relative linear velocity in x direction and control system set point respectively. In a similar manner an expression can be established for v_r.

Another way to implement the motion model is through dynamics. The 6 Degrees of Freedom (DOF) rigid body equations of motion described by Fossen [32] are

$$X = m[u^{\cdot} - vr + wq - x_G(q^2 + r^2) + y_G(pq - r^{\cdot}) + z_G(pr + q^{\cdot})] \tag{2.5}$$

$$Y = m[v^{\cdot} - wp + ur - y_G(r^2 + p^2) + z_G(qr - p^{\cdot}) + x_G(qp + r^{\cdot})] \tag{2.6}$$

$$Z = m[w^{\cdot} - uq + vp - z_G(p^2 + q^2) + x_G(rp - q^{\cdot}) + y_G(rq + p^{\cdot})] \tag{2.7}$$

$$\begin{aligned} K = {} & I_x p^{\cdot} + (I_z - I_y)qr - (r^{\cdot} + pq)I_{xz} + (r^2 - q^2)I_{yz} + (pr - q^{\cdot})I_{xy} \\ & + m[y_G(w^{\cdot} - uq + vp) - Z_g(v^{\cdot} - wp + ur)] \end{aligned} \tag{2.8}$$

$$\begin{aligned} M = {} & I_y q^{\cdot} + (I_x - I_z)rp - (p^{\cdot} + qr)I_{xy} + (p^2 - r^2)I_{zx} + (qp - r^{\cdot})I_{yz} \\ & + m[y_G(u^{\cdot} - vr + wq) - z_g(w^{\cdot} - uq + vp)] \end{aligned} \tag{2.9}$$

$$\begin{aligned} N = {} & I_z r^{\cdot} + (I_y - I_x)pq - (q^{\cdot} + rp)I_{yz} + (q^2 - p^2)I_{xy} + (rq - p^{\cdot})I_{zx} \\ & + m[x_G(v^{\cdot} - wp + ur) - y_g(u^{\cdot} - vr + wq)] \end{aligned} \tag{2.10}$$

The equations described above can be expressed in a more compact form:

$$M_{RB}\mathcal{V}^{\cdot} + C_{RB}(\mathcal{V})\mathcal{V} = \tau_{RB} \tag{2.11}$$

Here $\mathcal{V} = [u, v, w, p, q, r]^T$ is the body fixed linear and angular velocity and $\tau_{RB} = [X, Y, Z, K, M, N]$ is generalized vector of external forces and moments. M_{RB} is the rigid body inertia matrix and C_{RB} is Coriolis and centripetal matrix.

The right hand side of the vector 2.11 represents the external forces and moments acting on the vehicle. Fossen [32] classifies the forces into 1) Radiation-induced forces 2) Environmental Forces 3) Propulsion Forces. Table 2.2 shows the examples of various forces acting on an AUV.

Radiation Induced forces	Added Inertia, Hydrodynamic damping, Restoring Force
Environmental Forces	Ocean currents, Waves, Wind
Propulsion Force	Thruster/ Propeller Force, Control surface/ rudder force

Table 2.2: Examples of Forces acting on an AUV. Table taken from [32]

τ_{RB} can be represented as the sum of these forces.

$$\tau_{RB} = \tau_H + \tau_E + \tau \tag{2.12}$$

Here τ_H is the radiation induced forces and moments, τ_E is used to describe the environmental forces and moments and τ is the propulsion forces and moments. Equations 2.11 and equation 2.12 can be combined to yield the following representation of 6 DOF dynamic equations of motion:

$$M\mathcal{V}^{\cdot} + C(\mathcal{V})\mathcal{V} + D(\mathcal{V})\mathcal{V} + g(\eta) = \tau_E + \tau \tag{2.13}$$

where

$M \triangleq M_{RB} + M_A$; $C(\mathcal{V}) \triangleq C_{RB}(\mathcal{V} + C_A(\mathcal{V})$

M_A is the added inertia matrix $C_A(\mathcal{V})$ is the matrix of hydrodynamic Coriolis and centripetal terms. $g(\eta)$ is the restoring force. Equation **??** can ne used to calculate acceleration from the set of dynamic motion equations. Lammas [18] terms it as a navigation equation of the underwater vehicle.

$$\mathcal{V}^{\cdot} = M^{-1}(\tau - C(\mathcal{V})\mathcal{V} - D(\mathcal{V})\mathcal{V} - g(\eta)) \tag{2.14}$$

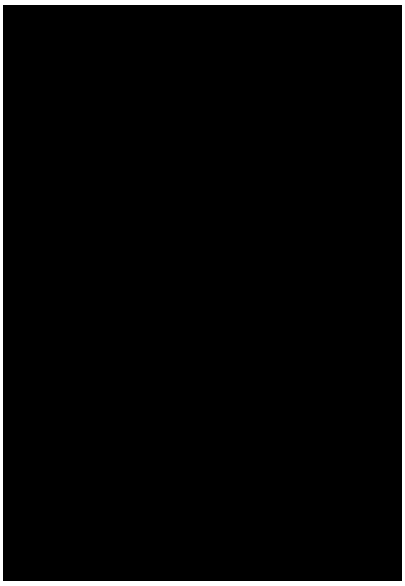

Figure 2.2: A temporal Bayesian model with hidden states x_t, observations z_t and controls u_t. Figure taken from [33]

2.2 Particle Filter

Particle filters is an integral part of my algorithm to learn the right parameters of a motion model and the way it is used is explained in rest of the section. A particle Filter is a state estimation algorithm based on a sampling method for approximating a distribution. Thrun [33] defines particle fitler as an alternative non-parametric implementation of the Bayes filter. It also can be called as a Sequential Monte Carlo(SMC) algorithm. The first attempt to use SMC was seen in simulations of growing polymers by M.N Rosenbluth and A.W. Rosenbluth [25]. Gordon et al. [11] provided the first true implementation of sequential Monte Carlo algorithm.

Thrun [33] stated that the key idea behind particle filter is to represent the posterior bel(x_t) by a set of random state samples drawn from this posterior. Instead of representing the distribution by a parametric form particle filter represents a distribution by a set of samples drawn from this distribution. In Figure **??** the belief is represented by a set of particles. The representation is a approximation but it is nonparametric and therefore there are advantages of using particle filters as an alternative to Extended Kalman Filter and Unscented Kalman Filter. Particle Filters can represent a broader space of distributions for example non-Gaussian and can model non linear transformations of random variables.

The objective of particle filters is to estimate the state of the system given the observation variables. They are designed for Hidden Markov Models(Fig 2.2), where the system consists of hidden and observed variables. In this model the state x_t is the hidden random variable as it is not directly observed. The state at time t is only dependent upon the state at time $t-1$ and external influences such as control u_t. The measurement z_t depends on the state at time t. The knowledge about the influence of the control on the system can be used to calculate a new expected location and the measurement can be combined in a Bayesian way.

The algorithm for particle filters is described below-:

Input: X_{t-1}: particle set

u_t: most recent control

z_t: most recent measurement

Output: X_t:particle set

begin

  for *m=1 to M do* **do**

    sample $x_t^m \sim p(x_t|u_t, x_{t-1}^m)$

    $w_t^m = p(z_t|x_t^m)$

    $X_t^- = X_t^- + (x_t^m, w_t^m)$

  end

  for *m=1 to M do* **do**

    draw i with probability $\propto w_t^{[i]}$

    add $x_t^{[i]}$ to X_t

  end

  return X_t

end

Algorithm 1: Particle Filter Algorithm. x_t^m is instatiation of the state at time t. X_t^- is a temporary particle set. M is the number of particles. Algorithm taken from [33]

In Algorithm 1 each particle x_t^m is instantiation of the state at time t. The first step is to generate a hypothetical state x_t^m for time t based on previous state x_{t-1}^m and control u_t. The particles are samples from the state transition distribution $p(x_t|u_t, x_{t-1})$. The importance factor for each particle x_t^m is calculated and denoted by w_t^m. Importance factor is defined as the probability of measurement z_t under the particle x_t^m. This probability is defined by a sensor model $p(z_t|x_t)$ Thus importance

Figure 2.3: Smoothing computes $P(X_k|e_{1:t})$, the posterior distribution of the state at some past time k given a complete sequence of observations from 1 to t. Figure taken from [27]

.

factor are used to incorporate the measurements into the particle set. In practice, the number of particles used are a large number(e.g.-:1000).

The key part of the algorithm is the re-sampling step in particle filter algorithm. The algorithm draws M particles with replacement from a temporary particle set X_t^-. The probability of drawing the particles is given by the importance factor. The re-sampling step is a probabilistic implementation of the Darwinian idea of survival of the fittest. It refocuses the particle set to regions in state space with high posterior probability.

2.3 Particle smoothing

The particle filter algorithm as described before is the first step in the Expectation process. The next algorithm that completes the Expectation Step is the particle smoothing. Doucet [7] in his paper stated that filtering based on observations received up to the current time is used to estimate the distribution of the current state of an Hidden Markov Model (HMM) whereas smoothing is used to estimate distribution of state at a particular time given all the observations up to some later time (Figure 2.3). Russel and Norving [27] showed that the state of the system is better estimated by smoothing as it incorporates more information than just filtering. We use particle smoothing algorithm proposed by Teddy N Yap and Christian R. Shelton [38] which was based on the technique presented by Docuet et al. [6] and Godsill et al. [10].

Particle smoothing is carried out in order to generate samples from the entire joint smoothing density $p(x_{0:T}|u_{1:T}, z_{1:T})$. The equations described by Yapp [38] are

$$p(x_{0:T}|u_{1:T}, z_{1:T}) = \prod_{t=0}^{T} p(x_t|x_{t+1:T}, u_{1:T}, z_{1:T}) \tag{2.15}$$

where,

$$\begin{aligned} p(x_t|x_{t+1:T}, u_{1:T}, z_{1:T}) &= p(x_t|x_{t+1}, u_{1:t+1}, z_{1:t}) && (2.16)\\ &= \frac{p(x_{t+1}|x_t, u_{1:t+1}, z_{1:t})p(x_t|u_{1:t+1}, z_{1:t})}{p(x_{t+1}|u_{1:t+1}, z_{1:t})} && (2.17)\\ &= \frac{p(x_{t+1}|x_t, u_{t+1})p(x_t|u_{1:t}, z_{1:t})}{p(x_{t+1}|u_{1:t+1}, z_{1:t})} && (2.18)\\ \alpha \quad & p(x_{t+1}|x_t, u_{t+1})p(x_t|u_{1:t}, z_{1:t}) && (2.19) \end{aligned}$$

Equation 2.19 is used to generate states backwards in time give future states. $p(x_{t+1}|x_t, u_{t+1})$ is the state transition probability and $p(x_t|u_{1:t}, z_{1:t})$ is obtained by performing particle filtering.

Algorithm 2 shows the step involved to sample from the entire joint smoothing density.

Input: $X_t, t = 0, 1, ..., T$: particle approximations to the posterior pdfs
$p(x_t|c_{1:t}, s_{1:t}), t = 0, 1, .., T$

$c_{1:T} = (c_1, c_2, ..., c_T)$: set of controls from time 1 to time T

Output: $x^{'}_{0:T} = (x^{'}_0, x^{'}_1, ..., x^{'}_T)$: a sample from the entire joint smoothing density $p(x_{0:T}|c_{1:T}, s_{1:T})$

begin
  draw i with probability $\propto w_T^{[i]}$ $x^{'}_T \leftarrow x_T^{[i]}$
  for $t \leftarrow T-1$ *down to 0 do* **do**
    for $i \leftarrow 1 to N_s$ *do* **do**
      $w_{t|t+1}^{[i]} \leftarrow w_t^{[i]} p(x^{'}_{t+1}|x_t^{[i]}, u_{t+1})$
    end
    draw i with probability $\propto w_{t|t+1}^{[i]}$
    $x^{'} \leftarrow x_t^{[i]}$
  end
end

Algorithm 2: Sample the entire joint smoothing density $p(x_{0:T}|c_{1:T}, s_{1:T})$

In the first step of the algorithm a particle is drawn with probability proportional to the filtered weight of the particles. The next step is to move a time step back and

modify the weights of the particles by calculating the new smoothed weights. The new smoothed weights are the product of state transition probability $p(x_{t+1}^{'}|x_t^{[i]}, u_{t+1})$ and the weight of the particle $w_t^{[i]}$. The next step in the algorithm is to draw particles with probability proportional to new smoothed weights $w_{t|t+1}^{[i]}$. The sequence of particles $x^{'}$ drawn from joint smoothing density $p(x_{0:T}|c_{1:T}, s_{1:T})$ from time 0 to time T form a sampled trajectory $x_{0:T}^{'} \triangleq (x_0^{'}, x_1^{'}, ..., x_T^{'})$.

Chapter 3

Learning the motion model

3.1 Introduction

The literature is full of different methods to calibrate a robot (eg-: [4] [37]). Virtually all the methods discussed before Roy's work [26] required human intervention and assumed the world to be static. These methods required a human to have experience and a device to measure the exact movement of a robot to calibrate. The most important assumption that these methods made was that the physics of a robot never changed and operated in a static environment.

Roy and Thrun first proposed an online self-calibration method [26] in 1999 that adapted to changes that occurred during the lifetime of a robot. The algorithm was designed for land robots where the final pose was given by equations described below

$$x^{'} = x + Dcos(\theta + T) \tag{3.1}$$

$$y^{'} = y + Dsin(\theta + T) \tag{3.2}$$

$$\theta^{'} = (\theta + T) mod 2\pi \tag{3.3}$$

D and T are the true translational and rotation of a robot. The measured translational and rotational is d and t and if robot's odometry is accurate then $D = d$ and $T = t$. In practice there is a difference and Roy represents D and T by equations 3.4 and 3.5 respectively.

$$D = d + \sigma_{trans} d + \epsilon_{trans} \tag{3.4}$$

$$T = t + \sigma_{rot} d + \epsilon_{rot} \tag{3.5}$$

ϵ_{trans} and ϵ_{rot} are the random variables with zero mean. σ_{trans} and σ_{rot} denote the systematic errors in the system. An example of such an error is drift. The

systematic errors referred here stay almost constant over a prolonged period of time. The algorithm they propose is used to estimate σ_{trans} and σ_{rot} using sensor data collected throughout robot's motion. They treat the problem as maximum likelihood estimation problem where the parameters are estimated under a dataset z as described in equation 3.6.

$$(\sigma^*_{trans}, \sigma^*_{rot}) = argmaxP(\sigma_{trans}, \sigma_{rot}|z) \tag{3.6}$$

Austin and Eliazar [8] proposed a different method to achieve the same goals proposed by Roy and Thrun. Their algorithm was different from Roy and Thrun for two reasons. Firstly, Austin ad Eliazar used a more general model which incorporated independence of motion terms. Secondly, the method was able to estimate parameters for non systematic errors as well. The motion model proposed by them to account is -:

$$\begin{aligned} x^{'} &= x + Dcos(\theta + T/2) \\ y^{'} &= y + Dsin(\theta + T/2) \\ \theta^{'} &= (\theta + T/2)mod2\pi \end{aligned} \tag{3.7}$$

As the turn and drive commands are performed independently therefore to not violate this assumption this model makes T reasonably small and it is absorbed as part of noise. To estimate non-systematic errors the true translational(D) and rotation(T) are represented by normal distribution with mean d and t and the variance will scale with d^2 and t^2 as shown in equation 3.8

$$\begin{aligned} D &\sim \mathcal{N}(d\mu_{D_d} + t\mu_{D_t}, d^2\sigma^2_{D_d} + t^2\sigma^2_{D_t}) \\ T &\sim \mathcal{N}(d\mu_{T_d} + t\mu_{T_t}, d^2\sigma^2_{T_d} + t^2\sigma^2_{T_t}) \end{aligned} \tag{3.8}$$

where μ_{A_b} is the coefficient for the contribution of odometry term b to the mean of the distribution over A. The algorithm is used to learn these set of mean and variances.

The method by Austin an Eliazar used EM framework to learn the parameters of the motion model for land robots. In the E step particle filtering and smoothing were performed to get a set of trajectories. In M step the maximum likelihood values of parameters given the trajectories was calculated.

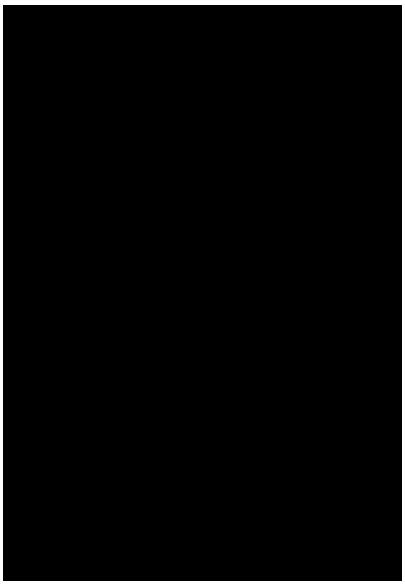

Figure 3.1: Block Diagram for the parameter estimation framework. Figure taken from [38].

Teddy Yapp [38] used the same framework and learned parameters for motion as well as sensor model of land robots (Figure 3.1). They adopted the same motion model but with slightly different noise model as shown in equation 3.9.

$$\begin{aligned} D \sim &\quad \mathcal{N}(d, d^2\sigma^2_{D_d} + t^2\sigma^2_{D_t} + \sigma^2_{D_1}) \\ T \sim &\quad \mathcal{N}(t, t^2\sigma^2_{T_d} + t^2\sigma^2_{T_t} + \sigma^2_{T_1}) \end{aligned} \tag{3.9}$$

The extra constant terms σ_{D_1} and σ_{T_1} are added to account for the errors that are not proportional to the translation or rotation of a robot.

Hegrenaes [14] in his work showed the importance of motion model for navigation in underwater vehicle. They proposed a novel approach for navigation systems in which knowledge about the vehicle dynamics was used to aid the Inertial Navigation System(INS). The new navigation system was tested on real dataset collected by an AUV.

For navigation in AUV velocity of the vehicle needs to be estimated and sensors such as IMU, DVL etc. are used. In a traditional INS system the key component is an IMU and a set of navigation equations. The reading from accelerometer and gyroscope are integrated to get an estimate of velocity, position and orientation. The reading from such sensors consist of inherent errors and leads to drift in the INS

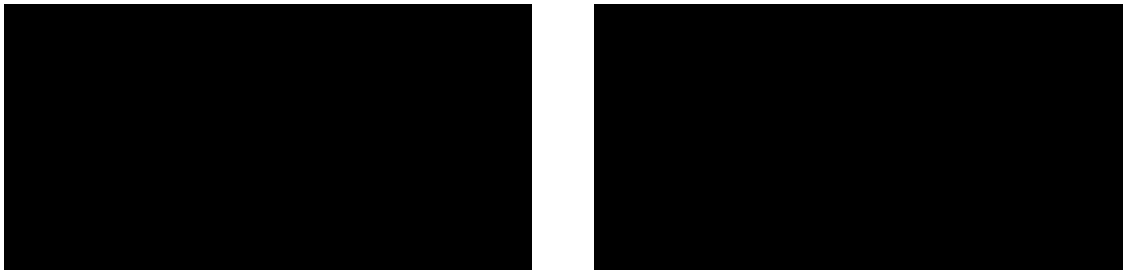

(a) Traditional aided INS (b) Model-aided INS

Figure 3.2: High level system outline. The vehicle model can be used in parallel to external aiding sensors. Figure taken from [14]

system. Generally sensors such as surface GPS, DVL etc. are an aiding system to the INS (Figure 3.2(a)). Combination of such systems leads to better estimate of velocity, position and orientation [20].

Hergreanaes [14] points out an alternative velocity information such as velocity estimate through vehicle dynamics is required because there are situations where it is not possible for the AUV to surface and get a GPS reading or DVL measurement needs to be discarded due to poor quality. The high level system outline for such a model is shown in Figure 3.2(b).

The system is very similar to traditional INS except that the vehicle model output in also integrated to the system. The vehcile model output doesn't require any extra instruments therefore can be easily applied to any vehicle. An alternative velocity estimate aids the INS where DVL readings are lacking as well as gives redundancy to the system.

All the above calibration methods are designed for odometric based motion models and for land robots. The use of vehicle model to aid the INS for navigation purposes shows us the importance of an adaptive motion model. The algorithm that I propose is for underwater vehicles and velocity based motion model. The process to adapt the motion model is similar to the previous work by Yapp and Eliazar and our approach is described in rest of the chapters.

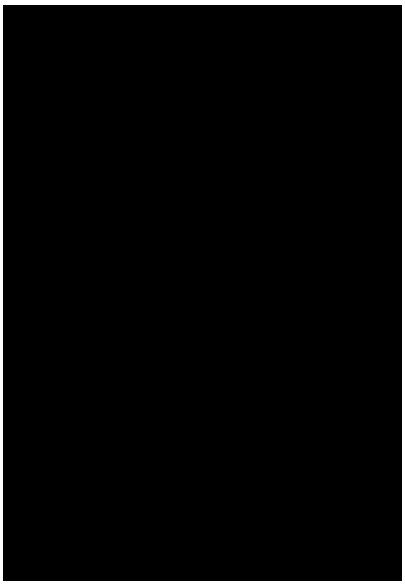

Figure 3.3: Block diagram for the algorithm proposed to adapt motion model.

3.1.1 General Architecture

In this section we give an overview of the system and point out the differences in my system as compared to the existing system proposed by Yapp [38]. Figure 3.3 is an outline of the proposed system. The motion and sensor models are initialized with a set of parameters. Given the motion model $p(x_t|x_{t-1}, u_t)$, sensor model $p(z_t|x_t)$ and the pose $p(x_{t-1})$ of a robot we can perform particle filtering using Algorithm 1. It is performed to estimate the pose $p(x_t)$ of a robot at the next time step.

The key ingredient to learn the motion model is to have an estimate of the ground truth. Particle smoothing (algorithm 2) is performed on the particle set produced by particle filtering to get an idea of ground truth. The algorithm can be repeated several times to get a set of trajectories. Particle filtering and smoothing are the key algorithm for the Expectation Step.

The reported translational and rotational movement of a robot is recorded for every time step. Based on the trajectories and reported movements the errors are calculated at each time step. After we have a set of errors, we perform Newton Conjugate gradient on the error function to estimate parameters. Conjugate gradient is an iterative method to solve large systems of linear equations [30]. This completes the Maximization Step.

The learned parameters are reassigned to the motion model and helps in adapting

our model to changes in robot and the environment. The whole algorithm is repeated at every time step so that we can dynamically learn the right parameters.

The system proposed for parameter estimation is similar to the system by Yapp [38]. I use the same EM framework and conjugate gradient to learn the right parameters for the model. The difference lies that the motion model learned is a velocity based motion model as compared to odometry based model. Secondly we use side sonar images to calculate landmarks on the fly for underwater environments. Therefore the algorithm doesn't rely on static maps for reference points.

3.2 Adapting Motion Model

3.2.1 Expectation Maximization

EM is an iterative process of finding maximum likelihood of parameters of a model which depend upon hidden variables. It is used to estimate unknown parameters θ given the observed data X. Z is the non-observed (hidden, latent) variable. In practice a complete dataset is not given and only a set of observations or incomplete dataset X is found. The hidden variables are important to a problem but complicate the learning process [27]. In order to learn with hidden variables Dempster et al. [5] proposed a method to maximize the probability of the parameters θ give the dataset X with hidden variables Z that he called as EM.

$$\theta^* = argmax_\theta \int p(\theta, Z|X)dZ \tag{3.10}$$

The key idea behind the EM algorithm is to alternate between estimating parameters θ and hidden variable Z. The E step consists of finding the posterior distribution of hidden variables $p(Z|X, \theta^{old})$ given the current estimate of parameters θ^{old}. The posterior distribution is used to find expectation of the data as shown in equation 3.11.

$$\mathcal{Q}(\theta, \theta^{old}) = \sum_Z p(Z|X, \theta^{old}) \ln p(X, Z|\theta) \tag{3.11}$$

In the M step we maximize the function as shown in equation 3.12 to estimate the new parameters θ^{new}.

$$\theta^{new} = argmax_{theta}\mathcal{Q}(\theta, \theta^{old}) \tag{3.12}$$

The objective as described by Minka [22] is to maximize $\mathcal{Q}(\theta, \theta^{old})$ and we want an updated estimate of θ^{new} such that

$$\theta^{new} > \theta^{old} \tag{3.13}$$

or we want to maximize the difference,

$$\mathcal{Q}(\theta^{new}) - \mathcal{Q}(\theta^{old}) = \ln P(X|\theta^{new}) - \ln P(X|\theta^{old}) \tag{3.14}$$

The above equations with hidden variables can be written as

$$\mathcal{Q}(\theta^{new}) - \mathcal{Q}(\theta^{old}) = \ln(\sum P(X|z, \theta^{new})P(Z|\theta^{new})) - \ln P(X|\theta^{old}) \tag{3.15}$$

Using Jensen's Equality it can be show that,

$$\ln \sum_{i=1}^{n} \lambda_i x_i \geq \sum_{i=1}^{n} \lambda_i \ln(x_i) \tag{3.16}$$

for constants $\lambda_i \geq 0$ with $\sum_{i=1}^{n} \lambda_i = 1$.
This can be applied to equation 3.15 and $\lambda = P(Z|X, \theta^{old})$. As $P(Z|X, \theta^{old})$ is a probability measure we have $P(Z|X, \theta^{old}) \geq 0$ and $\sum_Z P(Z|X, \theta^{old}) = 1$.

$$\begin{aligned}
Q(\theta^{new}) - Q(\theta^{old}) &= \ln(\sum_Z P(X|Z, \theta^{new})P(Z|\theta)) - \ln P(X|\theta^{old}) && (3.17)\\
&= \ln(\sum_Z P(X|Z, \theta^{new})P(Z|\theta).\frac{P(Z|X, \theta^{old})}{P(Z|X, \theta^{old})}) - \ln P(X|\theta^{old}) && (3.18)\\
&= \ln(\sum_Z P(z|X, \theta^{old})\frac{P(X|Z, \theta^{new})P(Z|\theta^{new}}{P(Z|X, \theta^{old})}) - \ln P(X|\theta^{old}) && (3.19)\\
&\geq \sum_Z P(Z|X, \theta^{old}) \ln(\frac{P(X|Z, \theta^{new})P(Z|\theta^{new})}{P(Z|X, \theta^{old})}) - \ln P(X|\theta^{old}) && (3.20)\\
&= \sum_Z P(Z|X, \theta^{old}) \ln(\frac{P(X|Z, \theta^{new})P(Z|\theta^{new})}{P(Z|X, \theta^{old})P(X|\theta^{old})}) && (3.21)\\
&\triangleq \triangle(\theta^{new}|\theta^{old}) && (3.22)
\end{aligned}$$

We continue by writing

$\mathcal{Q}(\theta^{new}) \geq \mathcal{Q}(\theta^{old}) + \triangle(\theta^{new}|\theta^{old})$

and for convenience define,

$q(\theta^{new}|\theta^{old}) \triangleq \mathcal{Q}(\theta^{old}) + \triangle(\theta^{new}|\theta^{old})$

The function $q(\theta^{new}|\theta^{old})$ is bounded by the likelihood functions $\mathcal{Q}(\theta^{new})$. We need to choose values of θ^{new} so that $\mathcal{Q}(\theta^{new})$ is maximized. The new updated value is denoted by θ_{n+1}.

$$\begin{aligned}
\theta_{n+1} &= argmax_\theta\{q(\theta^{new}|\theta^{old})\} && (3.23)\\
&= argmax_\theta\{\mathcal{Q}(\theta^{old}) + \sum_Z P(Z|X,\theta^{old}) \ln(\frac{P(X|Z,\theta^{new})P(Z|\theta^{new})}{P(Z|X,\theta^{old})P(X|\theta^{old})}\} && (3.24)\\
&= argmax_\theta\{\sum_Z P(Z|X,\theta^{old}) \ln(P(X|Z,\theta^{new})P(Z|\theta^{new})\} && (3.25)\\
&= argmax_\theta\{\sum_Z P(Z|X,\theta^{old}) \ln P(X,Z|\theta^{new})\} && (3.26)\\
& && (3.27)
\end{aligned}$$

We use the EM algorithm as described by Christopher M. Bishop[2] in his book. The steps taken in EM algorithm are described below -:

1. Have an initial estimate of the parameters θ^{old}
2. **E Step:** Evaluate $p(Z|X,\theta^{old})$
3. **M Step:** Evaluate $\theta^{new} = argmax_\theta L(\theta,\theta^{old})$

   where $L(\theta,\theta^{old}) = \Sigma_Z p(Z|X,\theta_{old}) \log p(X,Z|\theta)$
4. Check for the convergence of either the log likelihood or the parameter values. If the convergence criterion is not satisfied then let

   $\theta \leftarrow \theta^{new}$

   and return to step 2

In our algorithm we use Newton Conjugate Gradient to check for convergence and estimating the right parameters. Conjugate gradient is a method to determine the minimum or maximum of a function [30]. It is important to point that EM algorithm is local optimization technique and there are situations where it can get stuck in local optimum.

3.2.2 Parameter Estimation

In this section we give a detailed explanation of the method proposed to learn the motion model of a robot. As stated in Chapter 2.1 to calculate the position of an AUV we need to estimate velocity and feed it to the navigation equation 2.14. As we are operating in a dynamic environment various factors can lead to changes in

our motion model. To adapt the motion model we assume a Gaussian distribution to represent velocity. We assume it to be Gaussian as sum of several random noises leads to a such a distribution. Another assumption for the algorithm that we represent the pose of an AUV in two dimension as compared to six.

The velocity based motion model equations used are the following

$$x_t = x_{t-1} + V_{t-1}/W_{t-1}\sin(\theta_{t-1}) + V_{t-1}/W_{t-1}\cos(\theta_{t-1} + W_{t-1}\delta t) \tag{3.28}$$

$$y_t = y_{t-1} + V_{t-1}/W_{t-1}\cos(\theta_{t-1}) - V_{t-1}/W_{t-1}\sin(\theta_{t-1} + W_{t-1}\delta t) \tag{3.29}$$

$$\theta_t = \theta_{t-1} + W_{t-1}\delta t \tag{3.30}$$

where,

$$V \sim \mathcal{N}(v_t, v_t^2\sigma_{V_v}^2 + w_t^2\sigma_{V_w}^2 + \sigma_{V_1}^2) W \sim \mathcal{N}(w_t, v_t^2\sigma_{W_v}^2 + w_t^2\sigma_{W_w}^2 + \sigma_{W_1}^2) \tag{3.31}$$

The translational(V) and rotational(W) velocity are represented by a Gaussian distribution. The mean of the distributions are the reported translational v and rotational w velocity respectively. σ_{V_1} and σ_{w_1} are added to the motion model to account for errors that are not directly proportional to the translation and rotation of a robot.

Putting the whole problem of estimating parameters in EM framework, we define the parameters of the motion model that we want to learn are $\theta = \sigma_{V_v}^2, \sigma_{V_w}^2, \sigma_{V_1}^2, \sigma_{W_v}^2, \sigma_{W_t}^2, \sigma_{W_1}^2$ The data X from which the parameters can be learned is defined as $X = u_{1:T}, z_{1:T}$ where, $u_{1:T}$ and $z_{1:T}$ are the history of control and sensor readings. The robot's trajectory is the hidden variable in the system as it not directly observable and can be defined as $Z = x_{0:T}$.

The first step in an EM algorithm is to initialize the set of parameters θ with some initial values. In the E step we calculate the expectation of $\log p(Z, X|\theta)$ with respect to distribution $p(Z|X, \theta)$. The distribution can be represented by the entire join smoothing density $p(x_{0:T}|u_{1:T}, z_{1:T})$. To approximate the E step i.e. the joint smoothing density, particle filtering and smoothing is performed to calculate a set

of robot trajectories as discussed in section 2.3. In the M step we treat the set of trajectories as ground truth as use them to compute the maximum likelihood of parameters. The algorithm keeps on alternating between the E and M step until convergence.

For calculating the maximum likelihood values for parameters we need to calculate the motion errors $\epsilon_{V_t}, \epsilon_{W_t}$ based on robot trajectory and the contribution of translational v and rotational w velocity to the errors. The distribution that represents the errors are

$$\epsilon_{V_t}^{[j]} \sim \mathcal{N}(0, v_t^2\sigma_{V_v}^2 + w_t^2\sigma_{V_w}^2 + \sigma_{V_1}^2) \tag{3.32}$$

$$\epsilon_{W_t}^{[j]} \sim \mathcal{N}(0, v_t^2\sigma_{W_v}^2 + w_t^2\sigma_{W_w}^2 + \sigma_{W_1}^2) \tag{3.33}$$

where j is the index for each sampled trajectory.

The likelihood functions are

$$\mathcal{Q}_{\epsilon_D}(\sigma_{V_v}^2, \sigma_{V_r}^2, \sigma_{V_1}^2) = p(\tag{3.34}$$

$$epsilon_{V_v}^{[j]} \| u_{1:T}, z_{0:T}^{[j]}) \tag{3.35}$$

$$= \prod_j \prod_{t=0}^{T-1} \frac{1}{\sqrt{2\pi(v_t^2\sigma_{V_v}^2 + r_t^2\sigma_{V_w}^2 + \sigma_{V_1}^2)}} * \exp(\frac{(\epsilon_{V_t}^{[j]})^2}{2(d_t^2\sigma_{V_v}^2 + w_t^2\sigma_{V_w}^2 + \sigma_{V_1}^2)}) \tag{3.36}$$

$$\mathcal{Q}_{\epsilon_T}(\sigma_{W_d}^2, \sigma_{W_r}^2, \sigma_{W_1}^2) = p($$

$$epsilon_{W_t}^{[j]} \| u_{1:T}, z_{0:T}^{[j]})$$

$$= \prod_j \prod_{t=0}^{T-1} \frac{1}{\sqrt{2\pi(v_t^2\sigma_{W_v}^2 + w_t^2\sigma_{W_w}^2 + \sigma_{W_1}^2)}} * \exp(\frac{(\epsilon_{W_t}^{[j]})^2}{2(v_t^2\sigma_{W_v}^2 + w_t^2\sigma_{W_w}^2 + \sigma_{W_1}^2)})$$

The estimate the parameters we get the maximum likelihood estimates

$$\sigma_{V_v}^{2*}, \sigma_{V_r}^{2*}, \sigma_{V_1}^{2*} = argmax_{\sigma_{V_v}^2, \sigma_{V_r}^2, \sigma_{V_1}^2} \mathcal{Q}(\sigma_{V_v}^2, \sigma_{V_r}^2, \sigma_{V_1}^2) \tag{3.37}$$

$$\sigma_{W_d}^{2*}, \sigma_{W_r}^{2*}, \sigma_{W_1}^{2*} = argmax_{\sigma_{W_d}^2, \sigma_{W_r}^2, \sigma_{W_1}^2} \mathcal{Q}(\sigma_{W_d}^2, \sigma_{W_r}^2, \sigma_{W_1}^2) \tag{3.38}$$

We maximize the log likelihood function via Newton conjugate gradient method with respect to motion model parameters. In this method the gradient of the function is taken as the first search direction while the next search direction are chosen in such

a way that they are orthogonal to all previous search directions [30]. The gradient of log likelihood functions are

$$\mathcal{L}(\sigma^2_{V_v}, \sigma^2_{V_w}, \sigma^2_{V_1}) = -\frac{1}{2}\sum_j \sum_{t=0}^{T-1} [\log 2\pi + \log(v_t^2\sigma^2_{V_v} + w_t^2\sigma^2_{V_w} + \sigma^2_{V_1}) + \frac{(\epsilon^{[j]}_{V_t})^2}{v_t^2\sigma^2_{V_v} + w_t^2\sigma^2_{V_r} + \sigma^2_{V_1}}] \quad (3.39)$$

$$\mathcal{L}(\sigma^2_{W_v}, \sigma^2_{W_w}, \sigma^2_{W_1}) = -\frac{1}{2}\sum_j \sum_{t=0}^{T-1} [\log 2\pi + \log(v_t^2\sigma^2_{W_v} + w_t^2\sigma^2_{W_w} + \sigma^2_{W_1}) + \frac{(\epsilon^{[j]}_{W_t})^2}{v_t^2\sigma^2_{W_v} + w_t^2\sigma^2_{W_w} + \sigma^2_{W_1}}] \quad (3.40)$$

Chapter 4

Experimental Setup and Results

In this chapter we describe the experimental setup of the simulator to test our algorithm. To demonstrate the effectiveness of our approach the results from the simulated experiment are also shown.

4.1 Experimental Setup

To test our algorithm for learning the motion model we create a simulated world(Figure 4.1). The world size of our simulation is 400X400 with four landmarks shown in blue dots. The red $*$ shows the location of the robot and blue triangle is the location estimate of the robot by particle filters. The robot is moving with a constant forward and rotational velocity throughout the experiment. In simulation the robot can measure its distance from all four landmarks at all time. The sensor noise in the simulation can be varied in between the experiment. The particle size is 500 and is constant throughout the experiment. Table 4.1 shows the summary of variables for the experiment to test the effectiveness of our algorithm to learn a motion model.

	Experiment
World Size	400 units X 400 units
Total timesteps	200
No. of sensor readings	200
Translational Velocity	3 units/timestep
Rotational Velocity	0.1 degrees/timestep

Table 4.1: Summary of the experiments performed to adapt motion model.

At the start of the experiment the initial location of the robot and particle filters are randomly initialized (Figure 4.2(a)). The robot is moved by a constant velocity and Figure 4.2(b)(c)(d) shows the updated location of the robot as well as an estimate by particle filters of the robot's location.

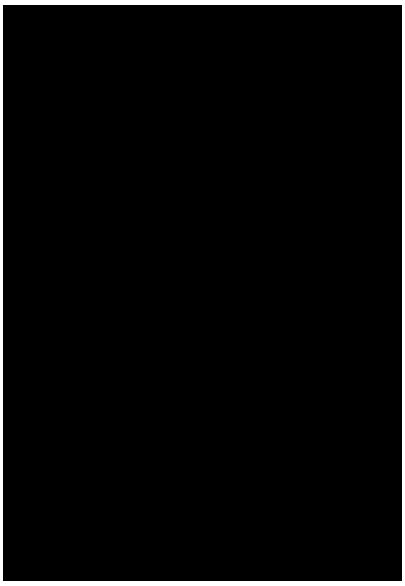

Figure 4.1: The simulation environment consisting of the robot(triangle) and the particle estimate of the location($*$). The blue dots represent the landmarks.

4.2 Results

In this section I describe the various experiments that were performed in the simulated world. The external changes in the envirorment were simulated by changing the parameters to arobot's motion model. The parameters can be altered by artificially introducing a drift in the motion or by changing the variance of the motion model distribution. As shown in Table 4.1 the total timesteps is 200 and in all the experiments we simulate the changes at time step 60.

As described in Chapter 2.1, the noise model for our simulated experiment is

$V_t \sim \mathcal{N}(v_t, v_t^2\sigma_{V_v}^2 + w_t^2\sigma_{V_w}^2 + \sigma_{V_1}^2)$

$W_t \sim \mathcal{N}(w_t, v_t^2\sigma_{w_v}^2 + w_t^2\sigma_{V_w}^2 + \sigma_{W_1}^2)$

In the first experiment we change $\sigma_{V_v}^2$ at time step 60 as shown in Table 4.2. The changed values of the parameter for the first and second case are 0.5 and 1.0 respectively. The number of trajectories is 3 and is kept constant for both cases. In this experiment we keep the sensor noise constant as well.

As shown in Table 4.2 the estimated value of $\sigma_{V_v}^2$ are 0.707 and 1.868 which are greater than the actual values and could lead to better localization. In order to demonstrate that, the localization error (euclidean error between the robot's actual position and location estimate of particle filters) is plotted for different times.

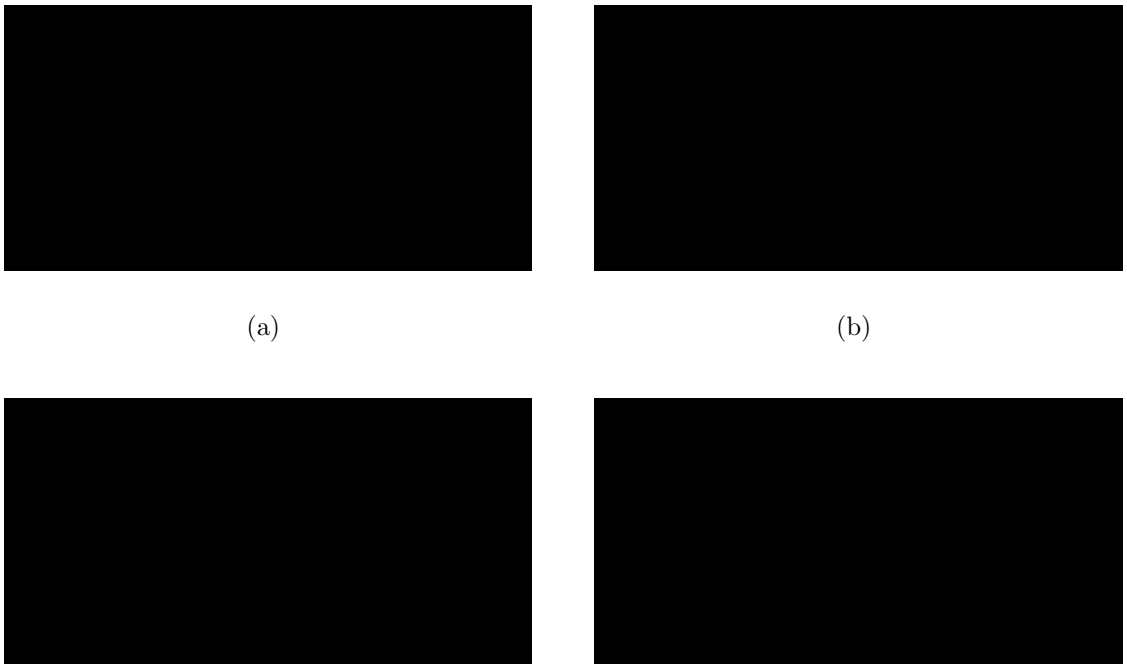

(a) (b)

(c) (d)

Figure 4.2: Particle Filters estimating the position of the robot. The robot is moved at a constant velocity of 5 units/timestep in each case. The particle filters estimate the location of the robot (star) by integrating the motion and sensor models.

Initial Parameter Values		Changed Parameter Values (after 60)		Estimated Parameter Values		Sensor Noise	Trajectories
		1	2	1	2		
$\sigma^2_{V_v}$	0.05	0.5	1.0	0.707	1.868	1.0	3
$\sigma^2_{V_w}$	0.05	0.05	0.05	0.05	0.05	1.0	3
$\sigma^2_{V_1}$	0.05	0.05	0.05	0.123	0.252	1.0	3
$\sigma^2_{W_v}$	0.05	0.05	0.05	1.476	1.496	1.0	3
$\sigma^2_{W_w}$	0.05	0.05	0.05	0.05	0.05	1.0	3
$\sigma^2_{W_1}$	0.05	0.05	0.05	0.208	0.210	1.0	3

Table 4.2: Initial and estimated values of parameters with constant sensor noise and trajectories

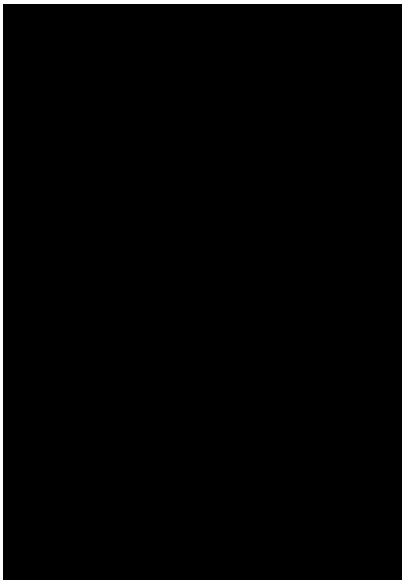

Figure 4.3: Plot showing the localization error between robot and the estimate of the robot's location by particle filters. The $\sigma^2_{V_v}$ is changed from 0.05 to 0.5 at timestep 60. The sensor noise is 1.0

In Figure 4.3 the red and blue line shows the error with a static motion model and adaptive motion model respectively. At the start of the experiment the parameter values for the robot's motion model and static motion model for particle filters are initialized with the same value. The adaptive motion model starts estimation the parameters from time step 0. In Figure 4.3 in the first 20 timesteps there is no change and we can see that the adaptive motion model performs better than the static. In theory the static motion model has the best estimate of robot' motion as

they are initialized with the same parameter value so the error should be less for static motion model. We don't see this because the location of particles are randomly initialized therefore it might be at different location to robot's start position. It needs the sensor model to decrease the error and as the sensor noise is high, it takes time to build the weight of particles. In the adaptive motion model to compensate for the sensor noise the distribution of motion model gets wider which helps in a better spread of the particle set.

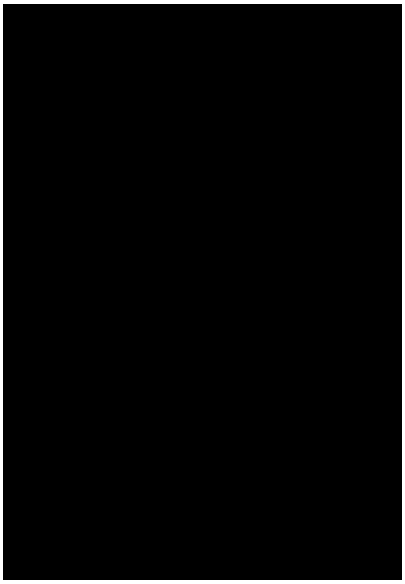

Figure 4.4: Difference between the maximum weight and average weight of the particle set. The motion model noise $\sigma^2_{V_v}$ is changed from 0.05 to 0.5 at timestep 60. The sensor noise is 1.0

In Figure 4.4 we plot the difference between the maximum weight and average weight of the particle set at each time step. This gives us an indication of the width of the distribution of the particle set. If we have a higher difference it means that the particle set contains particle which are sure about robot's location or vice versa. When the weights of particle are higher we can see the static motion model performing better. This is due to the resampling step of particle filters where they choose the most probable particles based on motion and sensor models. As soon as the algorithm starts picking the most probable particles, the error goes down. In the case of adaptive motion model the distribution of motion model gets wider right from the start which leads to higher difference thereby resulting in a decrease of localization error. After time step 60 we change the motion model noise and we can see that adaptive motion

model performing much better as compared to the static motion model. The difference in the weights of particles in Figure 4.4 also goes down.

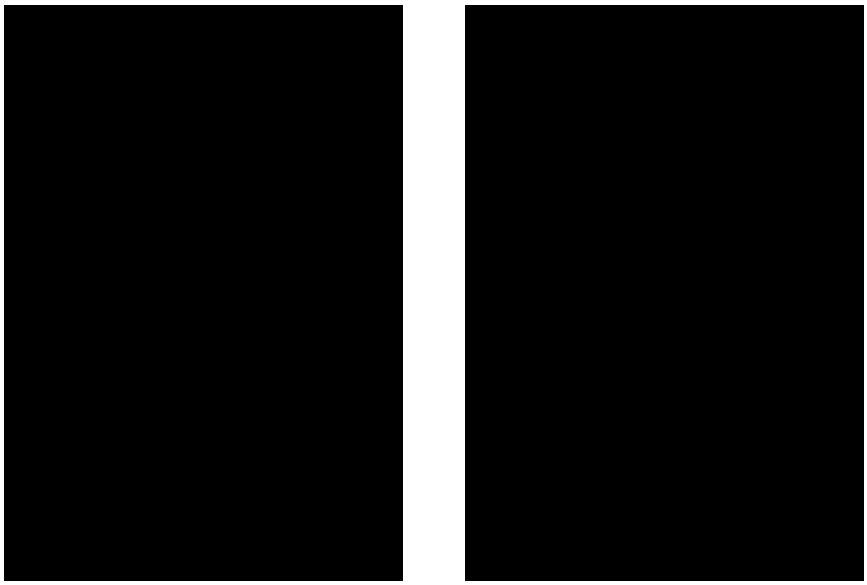

(a) (b)

Figure 4.5: Estimate of parameter values a) $\sigma^2_{V_v}$, $\sigma^2_{V_w}$, $\sigma^2_{V_1}$ b) $\sigma^2_{W_v}$, $\sigma^2_{W_w}$, $\sigma^2_{W_1}$ at every time step. The motion model noise $\sigma^2_{V_v}$ is changed from 0.05 to 0.5 at timestep 60. The sensor noise is 1.0

In Figure 4.7 we don't see a jump in the red line or green line at time step 60 and this due to the fact that the estimate of parameters before the change was greater than the change after time step 60.

In the next experiment $\sigma^2_{V_v}$ is changed from 0.05 to 1.0 and the errors, estimation of parameters and average weight are shown in Figure 4.6, Figure **??** and Figure 4.8 respectively.

In both the experiment's the robot's $\sigma^2_{V_1}$ is 0.05 and is not changed throughout the experiment. Table 4.2 shows that in the adaptive motion model the estimated value of $\sigma^2_{V_1}$ changes from the initialization value. Similarly other parameters such as $\sigma^2_{W_V}$ and $\sigma^2_{W_1}$ are also changed. This error in estimation is not of much concern as the main goal of the algorithm proposed was to learn the motion model to decrease the localization error.

In the first two experiments to simulate changes in the environment we changed

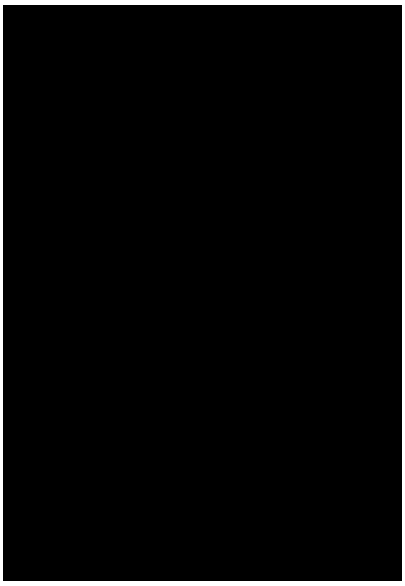

Figure 4.6: Plot showing the localization error between robot and the estimate of the robot's location by particle filters. The $\sigma^2_{V_v}$ is changed from 0.05 to 1.0 at timestep 60. The sensor noise is 1.0

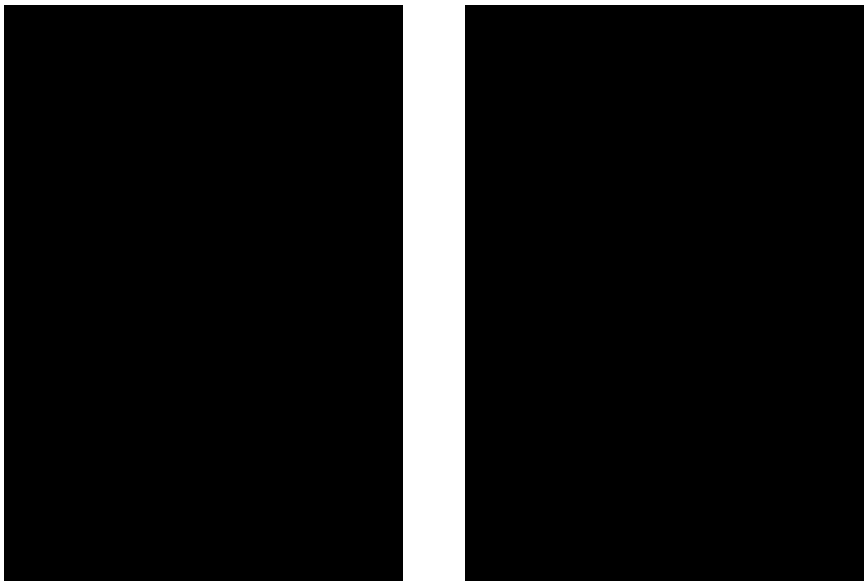

(a) (b)

Figure 4.7: Estimate of parameter values a) $\sigma^2_{V_v}$, $\sigma^2_{V_w}$, $\sigma^2_{V_1}$ b) $\sigma^2_{W_v}$, $\sigma^2_{W_w}$, $\sigma^2_{W_1}$ at every time step. The motion model noise $\sigma^2_{V_v}$ is changed from 0.05 to 1.0 at timestep 60. The sensor noise is 1.0

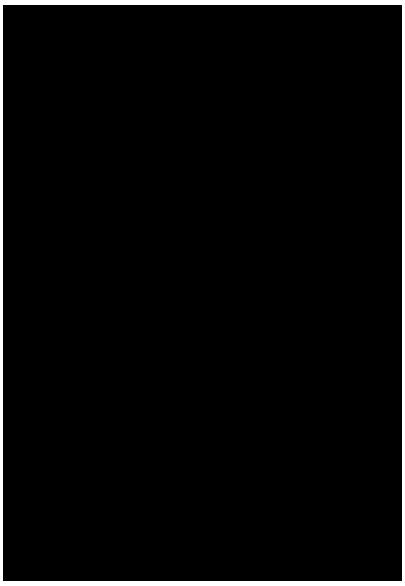

Figure 4.8: Difference between the maximum weight and average weight of the particles. The motion model noise $\sigma^2_{V_v}$ is changed from 0.05 to 1.0 at timestep 60. The sensor noise is 1.0

$\sigma^2_{V_v}$. In the next two experiments we induce drift in the system and compare both motion models in terms of localization error.

In order to simulate drift we describe the translational and rotational movement as

$$V_t \sim \mathcal{N}(v_t - a, v_t^2\sigma^2_{V_v} + w_t^2\sigma^2_{V_w} + \sigma^2_{V_1}) \tag{4.1}$$

$$W_t \sim \mathcal{N}(w_t - b, v_t^2\sigma^2_{w_v} + w_t^2\sigma^2_{V_w} + \sigma^2_{W_1}) \tag{4.2}$$

where a and b are constants representing drifts in the system.

Initial Parameter Values		Changed Parameter Values	Estimated Parameter Values	Drift	Trajectories	Sensor noise
$\sigma^2_{V_v}$	0.05	0.05	0.461	2.0	3	1.0
$\sigma^2_{V_w}$	0.05	0.05	0.05	2.0	3	1.0
$\sigma^2_{V_1}$	0.05	0.05	0.095	2.0	3	1.0
$\sigma^2_{W_v}$	0.05	0.05	1.460	2.0	3	1.0
$\sigma^2_{W_w}$	0.05	0.05	0.05	2.0	3	1.0
$\sigma^2_{W_1}$	0.05	0.05	0.206	2.0	3	1.0

Table 4.3: Initial and estimated values of parameters with drift

Table 4.3 gives a summary of the experiments performed to demonstrate the effectiveness of the algorithm to account for drift. To account for the drift we don't include an extra parameter in the motion model as the variances $\sigma_{V_v^2}$, $\sigma_{V_v^1}$ should account for drift and we see that in Table 4.3. The rest of the parameters remain unchanged.

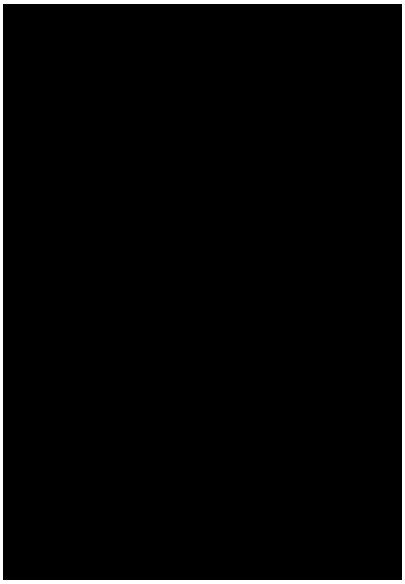

Figure 4.9: Plot showing the localization error between robot and the estimate of the robot's location by particle filters. The drift is present throughout the experiment described by equation 4.1 with a=2 . The rest of the parameters remain same and the sensor noise is 1.0.

The drift is present throughout the experiment. The performance of the algorithm is shown in Figure 4.9. The red line i.e. static motion model performs worse as compared to the adaptive motion model. The model adjusts its parameters as shown in Figure 4.10 to account for the drift in the system. The sensor model works to contain the drift in the system. Over time as it builds sufficient amount of particles to be confident of robot's location it then relocates the robot. This characteristic of sensor model leads to a sinusoidal pattern in red line.

Another way to include drift in the system is

$$V_t \sim \mathcal{N}(v_t * a, v_t^2\sigma_{V_v}^2 + w_t^2\sigma_{V_w}^2 + \sigma_{V_1}^2) \tag{4.3}$$

$$W_t \sim \mathcal{N}(w_t * b, v_t^2\sigma_{w_v}^2 + w_t^2\sigma_{V_w}^2 + \sigma_{W_1}^2) \tag{4.4}$$

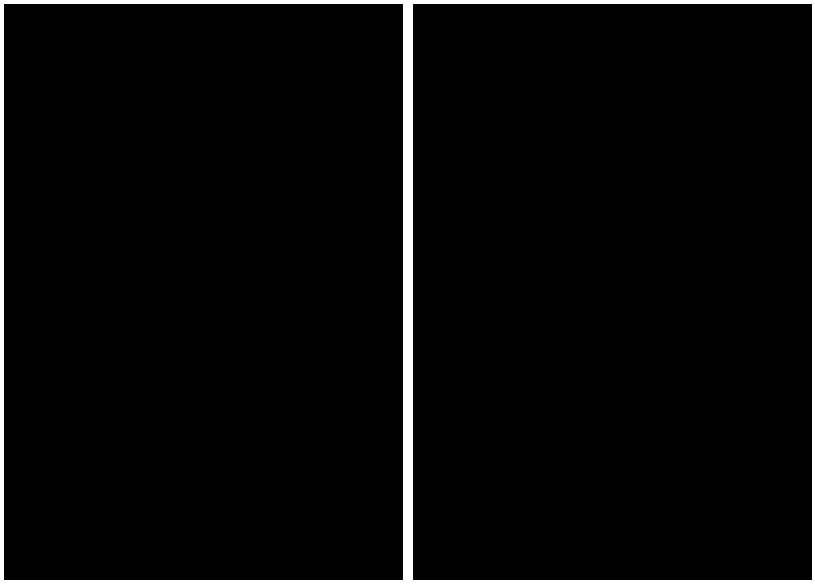

(a) (b)

Figure 4.10: Estimate of parameter values a) $\sigma^2_{V_v}$, $\sigma^2_{V_w}$, $\sigma^2_{V_1}$ b) $\sigma^2_{V_v}$, $\sigma^2_{V_w}$, $\sigma^2_{V_1}$ at every time step. The drift is present throughout the experiment described by equation 4.1 with a=2 . The rest of the parameters remain same and the sensor noise is 1.0.

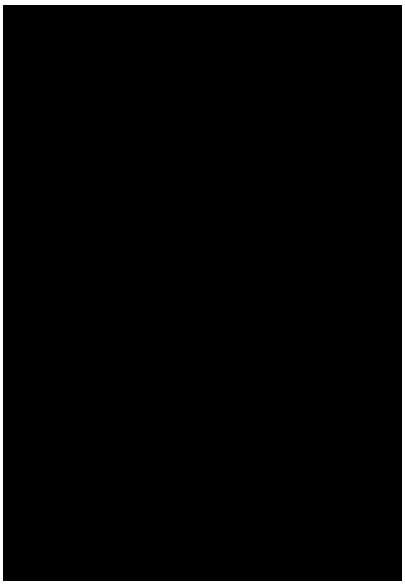

Figure 4.11: Plot showing the localization error between robot and the estimate of the robot's location by particle filters. The drift is present throughout the experiment described by equation 4.3 with a=2. The rest of the parameters remain same and the sensor noise is 1.0.

The results are described in Figure 4.11 and in this case as well the drift is present throughout the experiment. The static motion model performs worse as compared to adaptive motion model. In figure we can see the red line coming down for a short time as the robot gets relocated based on sensor model's estimate.

In all the experiments above we assume that the sensor noise is constant through out the experiment. In real world experiments we find that the quality of sensor readings varies with environment. For example, in an AUV we won't get sonar readings throughout the mission. This could be because sometimes its difficult to find the bottom of the sea floor or sonar sensor could be switched off for some time periods to save power on the battery.

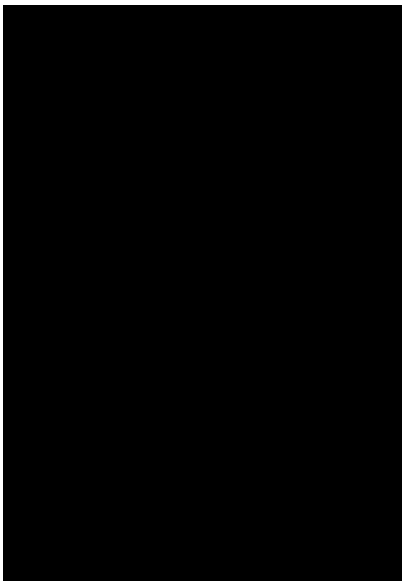

Figure 4.12: Plot showing the localization error between robot and the estimate of the robot's location by particle filters. The $\sigma^2_{V_v}$ is changed from 0.05 to 1.0 at timestep 60. The sensor noise is changed from 1.0 to 10.0 at timestep 100.

In the next experiment there are two changes at time steps 60 and 100. At time step 60 we change the motion model noise $\sigma^2_{V_v}$ from 0.05 to 0.5. We change the sensor noise at time step 100 and compare the behaviour of static and adaptive motion model. After time step 100 we can see the error growing in adaptive and static motion model. The adaptive motion model quickly learns the sensor noise is high and starts relying on its motion model. This helps in decreasing the localization error and can be seen in Figure 4.12. In learning with a high sensor noise we are adjusting

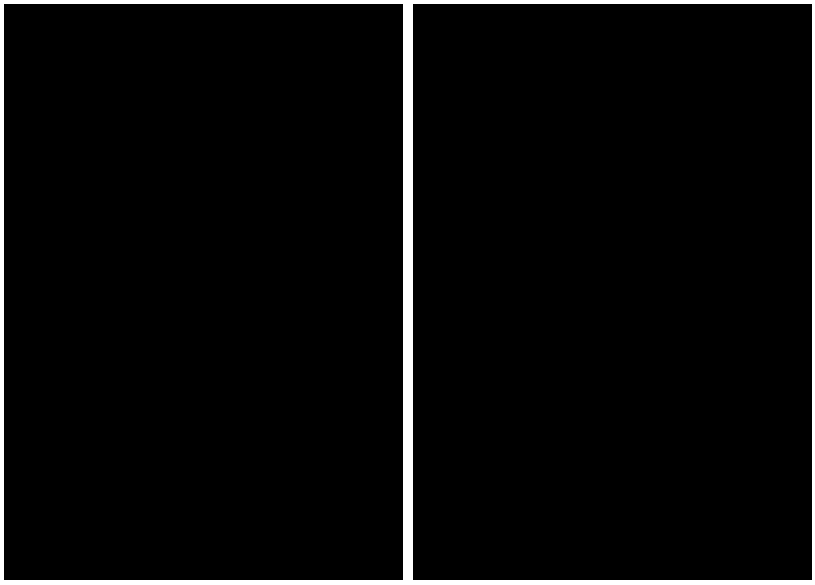

(a) (b)

Figure 4.13: Estimate of parameter values a) $\sigma^2_{V_v}$, $\sigma^2_{V_w}$, $\sigma^2_{V_1}$ b) $\sigma^2_{W_v}$, $\sigma^2_{W_w}$, $\sigma^2_{W_1}$ at every time step. The $\sigma^2_{V_v}$ is changed from 0.05 to 1.0 at timestep 60. The sensor noise is changed from 1.0 to 10.0 at timestep 100.

our motion model to compensate for the noise in the sensor model therefore we see an increasing estimate of the parameters (Figure 4.13).

In this chapter we have shown results for both static and adaptive motion model. In all the cases tested in my thesis the adaptive motion has performed better. The localization error was less in adaptive as compared to static motion model. In the adaptive motion model the estimates of motion model parameters were bad. The parameters estimates take into account the noise in sensor model. Therefore we don't see the estimated parameters being highly accurate. At the same time this helps in small localization error even with high sensor noise.

Chapter 5

Landmarks extraction using Side Sonar Images

5.1 Introduction

The sensor model $p(z_t|x_t)$ is the probability of a measurement z given the robot is at position x. Thrun [33] divides the sensors for mobile robots in five classes which are contact sensors, internal sensors, proximity sensors, visual sensors and satellite-based sensors. Examples for various classes are shown in Table 5.1.

Classes of Sensors	**Examples of each class**
Cpntact Sensors	Bumpers
Internal Sensors	Accelerometers, Gyroscopes, Compasses
Proximity Sensors	Sonar, Radar, Laser range-finders, Infra-red
Visual Sensors	Cameras
Satellite Based Sensors	GPS

Table 5.1: Sensors for Mobile robots. Table taken from [33]

The measurements from these sensors in a particle filter algorithm are used to assign weights aka importance factor to particles. Most common way of sensing the environment is through landmarks. The sensors measure the distance, bearing or both from the landmarks to estimate their position in the environment.

In our simulated experiment the sensor model assumes to have four static landmarks and at all times we can measure the distance from them. For our algorithm to work on AUV we need some sort of reference points to measure the actual movement of the vehicle. These reference points need to be computed on the fly as we don't have the luxury of having static maps for underwater environments. As my algorithm targets cases in which AUV doesn't loop back and we have limited field of view we need dynamic landmarks for our sensor model. To extract dynamic landmarks we used side sonar images and run feature extraction techniques such as SIFT on the images. These extracted landmarks can be used as reference points for our algorithm to adapt motion model for AUV.

The dynamic landmarks algorithm for side sonar images is not integrated in the simulated experiment described in Chapter 4. This is because of the unavailability of the motion data such as recording of IMU, DVL etc for AUV. To validate our algorithm for dynamic landmarks we extract motion information from real side sonar data and compare it to the total distance moved by the AUV. In the next two section I describe side scan sonar and SIFT. In section 5.2 the algorithm to compute landmarks is presented. Chapter 6 contains the results of the algorithm.

5.1.1 Side Scan Sonar

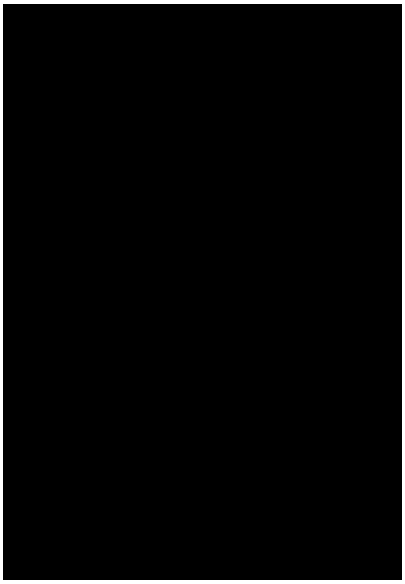

Figure 5.1: Side scan sonar sensor using dual frequency made by JW Fishers . Image taken from [9]

Side scan sonar is used to create pictures or an image of the sea floor. Sound waves travel very effectively in water as compared to light therefore at lower depths sonar is used to image the sea floor instead of cameras. A side scan sonar sensor is shown in Figure 5.1. It measures how "loud" the return echo is and computes a picture 5.2. In the sea floor there are hard areas such as rock and soft areas such as sand. The hard areas are represented by darker areas in the image as they return a stronger signal as compared to a soft area. A typical side sonar image is shown in Figure 5.2. Side scan sonar is the only imaging tool that works at low depth therefore we use it to extract landmarks for adapting the motion model.

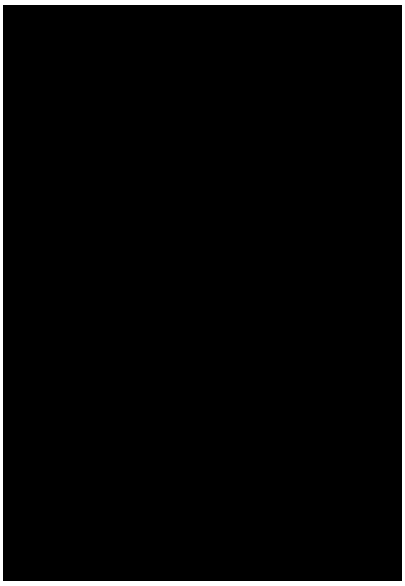

Figure 5.2: Side scan sonar image of the wreck. Image taken from [23]

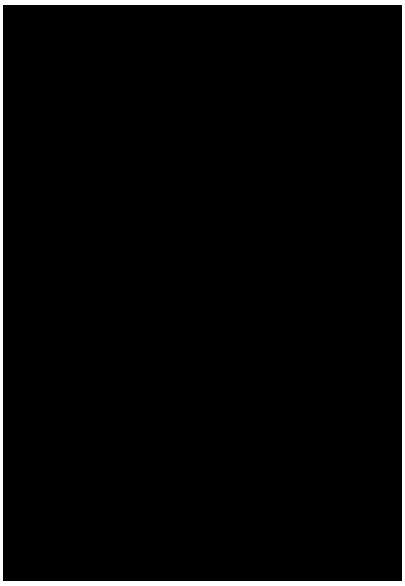

Figure 5.3: Working of a side scan sonar. Image taken from [23]

Side-scan transmits sound energy and analyses the echo that is bounced off from the sea floor or other objects. It typically consists of three basic components: towfish, transmission cable and topside processing unit. It emits pulses in the shape of cone or fan to either sides of the towfish, typically to a distance of 100 meters. The angular dimensions of these beams are designed to be narrow along-tack and wide across track to cover as much seabed range as possible. The echoed sound waves are received by

Sidescan Sonar Type	Frequency	Wavelenght	Range
"Low"	5 kHz	30 cm	¿50 km
"Low"	10 kHz	15 cm	10 km
"Low"	25 kHz	6 cm	3 km
"Medium"	50 kHz	3 cm	1 km
"Medium"	100 kHz	1.5 cm	600 m
"Medium"	200 kHz	0.75 cm	300 m
"High"	500 kHz	3 mm	150 m
"High"	1 mHz	1.5 mm	50 m

Table 5.2: Characterization of Sidescan system according to their operating frequency. Table taken form [34]

transducers and are continuously recorded. Each pulse shows a narrow strip below and to the sides. The recorded echos are put together along the direction of motion to form images of the seafloor. The sound frequencies range from 100 to 500 Khz in side scan sonar; higher frequencies yield better resolution but less range. Currently in the market there are systems with dual frequency which allow the operator to use high frequency to produce sharper images or lower frequencies to cover greater depths. Side scan systems can be characterized according to their operating frequency [34].

Sonar are useful instruments in fisheries research, environmental studies and military applications such as mine detection.

5.1.2 SIFT

SIFT is a popular algorithm in computer vision to detect and describe local feature of an image that are not affected by scaling and rotation. It was proposed by David Lowe in 1999 [21] and has been used for object recognition, robotic mapping and navigation, image stitching, video tracking and others. The various steps for extracting SIFT feature as described by David Lowe are explained in this section.

The first step in SIFT algorithm is to construct scale space i.e. create internal representations of the original image to ensure scale variance. In SIFT, progressively blurred out images are generated using the original image. In next step you the original image is resized to half of its size and again blurred out images are generated.

Images of same size are grouped together and belong to an octave. In Figure 5.4 there are four octave and each octave has five images. The number of octaves depends

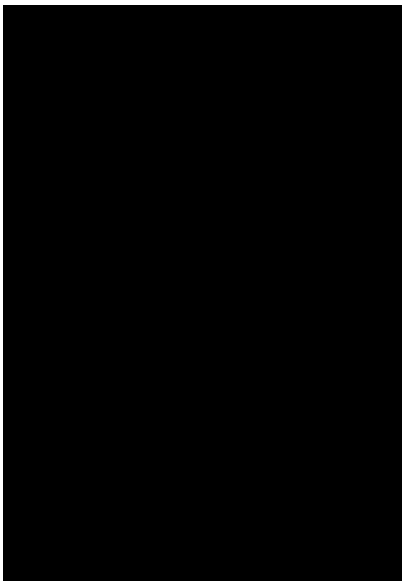

Figure 5.4: Representation of what Octaves look like in SIFT. Image taken from [35]

upon the original size of the image. The blurring of images in each octave can be represented mathematically by

$$L(x, y, \sigma) = G(x, y, \sigma) * I(x, y) \tag{5.1}$$

where L is the blurred image, G is the Gaussian blur operator, I is an image, x,y are the location coordinates and σ is the scale parameter. The symbol $*$ represents the convolution operator. The next step is to find another set of images by Difference of Gaussian (DOG) which finds out interesting keypoints in the image. In this step the difference between two consecutive scales is calculated as shown in Figure 5.5. This process is done at every octave.

As an example the DOG is applied to cat images and the output is shown in Figure 5.6.

After calculating the DOG images we can find the keypoints in two steps. We first locate the maxima/minima in DOG images. Secondly find subpixel maxima/minima. In the first step the algorithm iterates through each pixel and all the neighbors are checked. This process is explained in Figure 5.7

In Figure 5.7 X is the current pixel and the green circles represent the neighbors. X is marked as a keypoint if it is the greatest or least of all neighbours. These are approximate as mostly the maxima/minima never lies on a pixel. To access the data

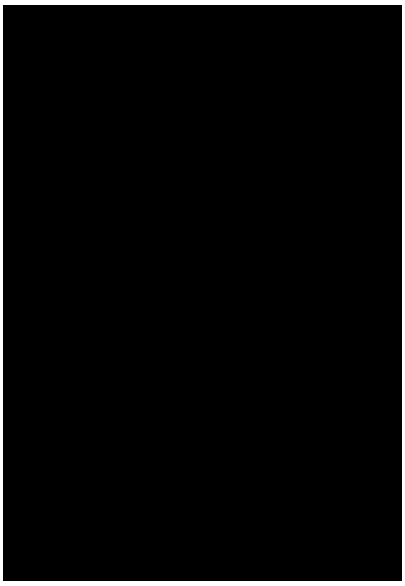

Figure 5.5: Difference of Gaussian done to caluclate keypoints in the image. Image taken from [35]

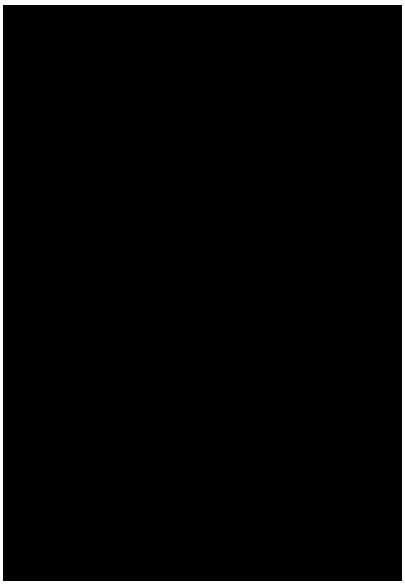

Figure 5.6: Applying DOG on a set of images present in a single octave. Image taken from [35]

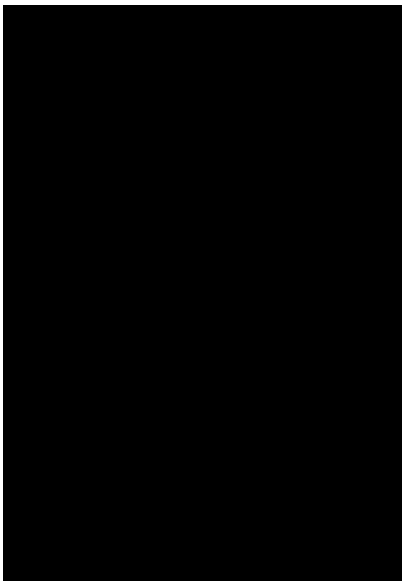

Figure 5.7: Locate maxima/minima in DOG images. X marks the current pixel and it is compared with its 26 neighbours. Image taken from [35]

"between" pixels we need to calculate the subpixel location. This can be done by Taylor expansion of the image around the approximate keypoint.

After generating a set keypoints we need to eliminate points which have low contrast features and are present on an edge. The algorithm checks for intensity value at the pixel location of the keypoint and if it is less than a certain value if is rejected. To remove edges the perpendicular gradients are calculated at the keypoint. If both the gradients are small it is a flat region. If one gradient is big and other is small it is an edge. If both the gradients are big then it is a corner. The keypoints with both big gradients are considered to be a keypoint otherwise they are rejected. The SIFT algorithm can check if a point is a corner or not by using a Hessian matrix. After completing this step we have a set of legitimate keypoints which are scale invariant. The next step is assign orientation to each keypoint so that they are rotation invariant.

In this step, SIFT calculates gradient magnitudes and directions around each keypoint. To perform this, a histogram is created with 36 bins (each 10 degrees) representing 360 degrees of orientation. Suppose the gradient direction at a certain point is 20.56 degrees then it will go in 20-29 degree bin. The amount that is added to the bin is proportional to the magnitude of the gradient of the point. This process

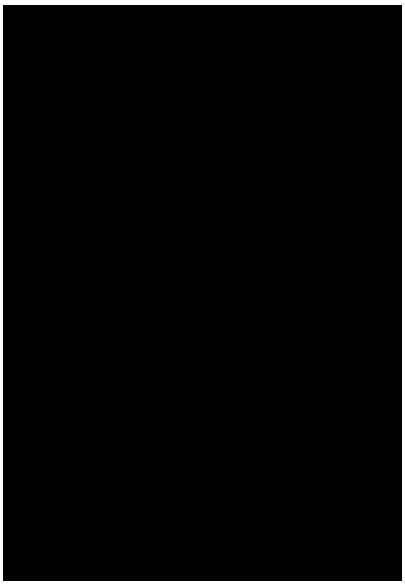

Figure 5.8: Histogram describing the bins for assigning orientation to the keypoint. Image taken from [35]

is repeated for all the pixels around the keypoint and the maximum bin is used to describe the keypoint. In Figure 5.8 it peaks at 20-29 degrees therefore the keypoint is assigned to third bin. In the Figure we also see that there is another peak which is above 80% of the highest peak. In this case the peak converted into a new keypoint. This new keypoint has the same location and scale as the original but has a different orientation.

In the final step of the SIFT algorithm, a unique fingerprint for a keypoint aka descriptor is calculated. To calculate the gradient we take 16×16 window around the each keypoint. This 16×16 window is broken into sixteen 4×4 windows (Figure 5.9).

In each window gradient magnitudes and orientations are calculated and are put in a 8 bin histogram (Figure 5.10). For examples a gradient orientation in the range of 0-44 degrees is put in the first bin. The amount added to the bin depends upon the magnitude of the gradient and the distance from the keypoint. The gradients that are far away from the keypoint will add smaller values to the bin. This can be performed using "Gaussian weighting function".

This is done for all 16 pixels, therefore we end up with $4 \times 4 \times 8 = 129$ numbers. The numbers are normalized and form the feature vector. This feature vector gives

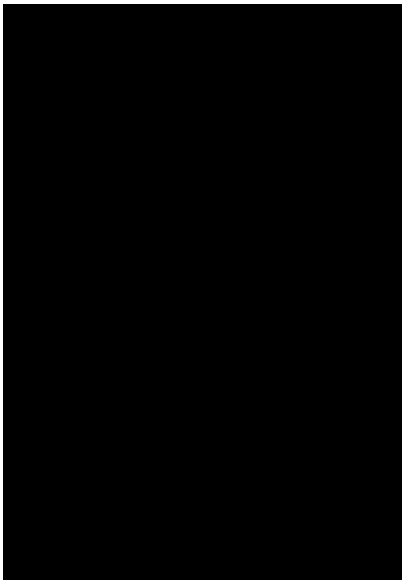

Figure 5.9: A 16×16 window is taken around a keypoint. This window is broken into sixteen 4×4 windows. Image taken from [35]

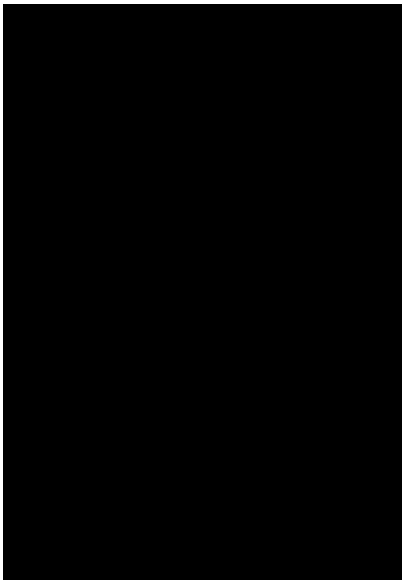

Figure 5.10: The gradient orientation is assinged to 8 bin histogram. The value depends upon the magnitude of the orientation and distance from the keypoint. Image taken from [35]

a unique identity to the keypoint. To achieve rotation independence, the keypoint rotation is subtracted from each orientation. Therefore each gradient orientation is relative to the keypoints orientation. For illumination independence we threshold any numbers that are big and the resultant feature vector is normalized again.

After we calculate the descriptors for each keypoint, we have a set of features that describes the image and these can be used for various image processing tasks such as image matching, stitching etc.

SIFT has been widely used in various robotic applications. Stephen Se et.ãl [29] proposed an vision based algorithm to localize a robot and map the environment using SIFT features. Various algorithm have been proposed to estimate motion from camera images using SIFT features [1] [28]. Similar algorithms have been proposed to estimate motion underwater using camera images [31].

SIFT has been compared to self-organized features from restricted Boltzmann machines(RBM) in Hollensen [**?**]. Vardy et.ãl [36] compared various image registration techniques for side sonar images such as maximization of mutual information, log-polar cross-correlation, SIFT and phase correlation. He presented results and concluded that SIFT and phase-correlation provide the best performance among all the techniques. Peter King [17] described an algorithm to generate images from side scan sonar pings in real time. There implementation can be used as a black box to my algorithm.

5.2 Dynamic Landmarks

As stated above we need reference points to adapt our motion model. These reference points need to be dynamic as we are learning online and we don't loop back on AUV's route. To generate landmarks on side sonar images a preprocessing step is required to get rid of horizontal lines produced spurious electrical noise in the transducers. The noisy side sonar images is shown in Figure 5.11.

The preprocessing step involves using a median filter on the image to get rid of the noise. The preprocessed image is shown in Figure 5.12.

The disadvantage of this step is that we loose information because the image is blurred. The blurred image won't give us meaningful keypoints therefore in the preprocessed image we see some horizontal lines due to restricted use of the filter. In

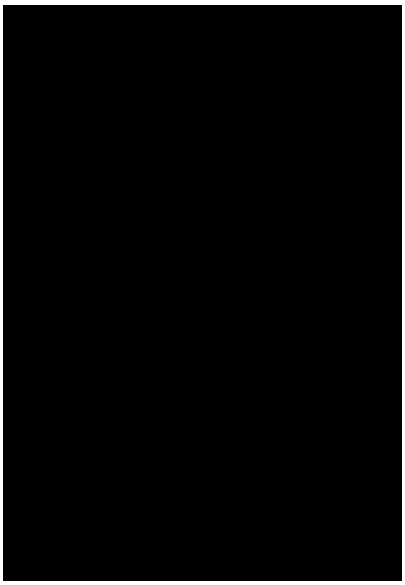

Figure 5.11: Image produced by Side scan sonar. Images produced from dataset provided by DRDC.

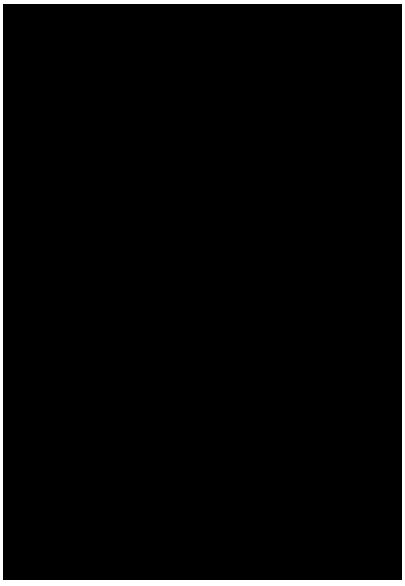

Figure 5.12: Median filter applied to side sonar image.

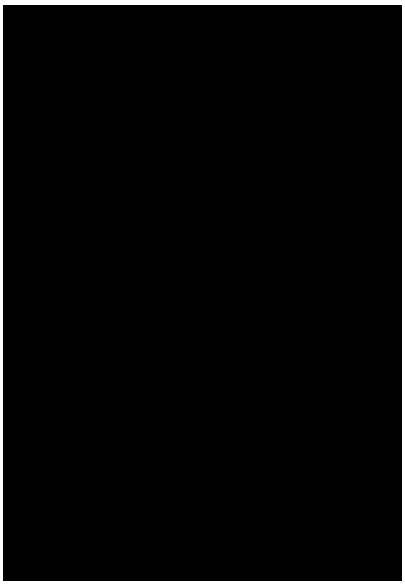

Figure 5.13: Median filter with high size applied to side sonar image.

order to get rid of all the lines we can increase the size of filter but the image will be very blurred as shown in Figure 5.13.

The preprocessed image is used to extract landmarks for the AUV. To generate landmarks we use feature extraction techniques such as SIFT. Figure 5.14 shows the keypoints generated by SIFT using a high Hessian threshold. These keypoints can be used as landmarks to adapt our motion model. We need to keep in mind that we need a high Hessian threshold or else the algorithm will generate hundreds of landmarks as shown in Figure 5.15.

The distance of the AUV to landmarks in x-y plane can be measured. Similarly the distance of the particle filter estimate to the landmarks can be measured. Both the measured distances can be compared and used to assign weights to the particles.

Using dynamic landmarks allows our adaptive motion model algorithm independence from a static map and helps us in learning on the fly.

5.3 Motion Estimation using side sonar images

In many advanced land-based robots the position and orientation is determined through wheel encoders and velocity estimates. These techniques do not generalize well as they cannot be applied every robot as well as the estimates drift over time.

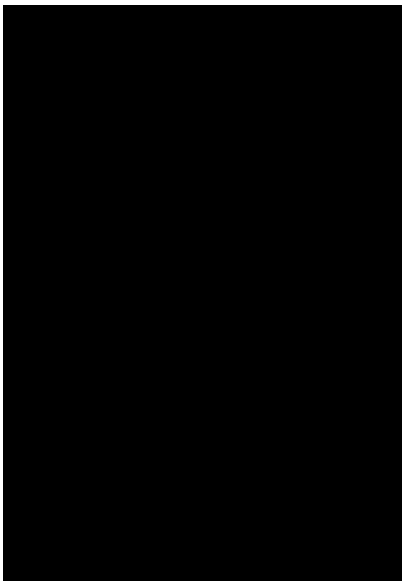

Figure 5.14: SIFT features on a side sonar image.

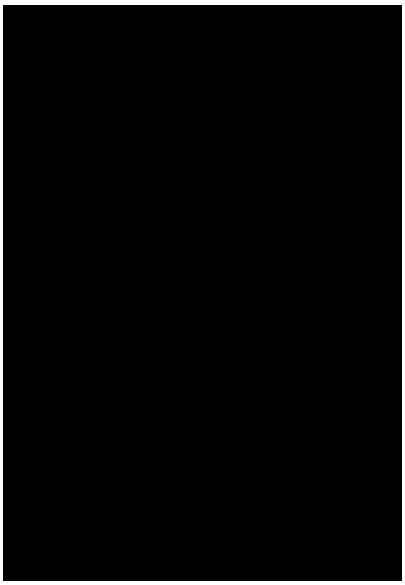

Figure 5.15: SIFT features on a side sonar image with low hessian threhold.

Motion estimation using visual sensors such as camera are not restricted to particular locomotion and doesn't suffer from drift. There has been a lot of work done in estimating motion using camera images on land robots [1] [28]. Silvia [31] proposed an algorithm for AUV which used camera images and SIFT to estimate motion.

Hegreneas [15] combined the knowledge of vehicle dynamics to aid INS systems. In a similar manner visual motion information can be used to aid INS systems. The visual input to the dead reckoning algorithm has its pros and cons. The main advantage of using a visual estimate is that it doesn't suffer from drift which is prime concern for underwater vehicles. The disadvantage lies in the fact that we don't have side sonar images available every time. The second disadvantage is the computation power available on AUV. To specifically deal with the problems we use a high Hessian threshold to extract maximum of 4 landmarks so that feature matching is not computationally expensive.

We verify our dynamic landmark approach by estimating motion information from side sonar images and compare it to reported movement by DVL. To generate keypoints we run SIFT on the side sonar images. We use a high Hessian threshold so that we can restrict the amount of keypoints. These keypoints are matched with keypoints of the next consecutive image using a KNN based matcher. This matcher is based on k-nearest neighbour based algorithm. As the name suggest the object is classified according to its k-nearest neighbours. Figure 5.16 shows two consecutive images that are used to estimate motion of the AUV. In the first image the keypoints are marked in white circles. These keypoints are matched with the second image and the matched keypoints are marked in black circles. The x and y position of the matched keypoints is compared to the original keypoints. This gives us motion estimate of the AUV.

The method to estimate motion is a very simple one with assumptions that AUV moves in a straight line at the same depth. The method proposed in the section was to verify the dynamic landmark approach instead of proposing an algorithm for estimating motion.

The performance of the algorithm is evaluated on real side sonar data. The results of the algorithm are compared to real motion information of the AUV and are discussed in the next chapter.

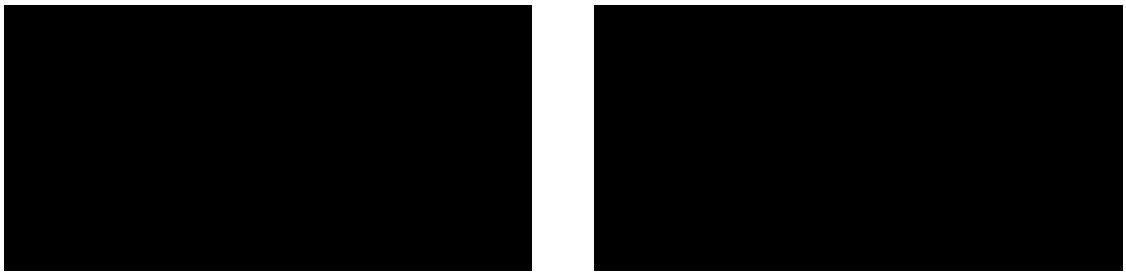

(a) a (b) b

Figure 5.16: Two consecutive side sonar images. The white circles represent the landmarks and the black circle in next image shows the matched keypoints.

Chapter 6

Results

6.1 Motion estimation using side sonar images

We validate our algorithm on datasets consisting of side sonar images and the total distance the AUV moves. The datasets are provided by Defence Research and Development Canada(DRDC). The SIFT features that are applied to side sonar images are implemented using popular vision library(Opencv) in python. The motion estimation algorithm and feature matching is also implemented in python. The video datasets provided could only be read by a specific software called sonar data reader. To test our algorithm we extracted a set of images from the video and used it as an input to our motion estimation algorithm. Table 6.1 shows the results of motion estimation using side sonar images. The table also shows the estimated distance by AUV using a DVL. The distance estimated by DVL can be noisy but is treated as ground truth because there is no practical noise free way to measure how much the AUV actually moved. The algorithm gives us a decent estimate of the movement. The results when compared to DVL data show that the algorithm to estimate motion from side sonar data was not extremely accurate. Its hard to judge whether the algorithm was at fault or the ground truth was noisy. Secondly the movement from side sonar images can be coupled with DVL through a Kalman filter to give a better estimation of the movement. Hegeranes [14] in his paper pointed out the use of external sensors to aid INS and estimation of movement from side sonar images can be used to contain the drift inherent in INS systems. The results presented shows the accuracy of our motion estimation algorithm.

Datasets	Distance estimated by DVL(m)	Distance estimated through Side sonar images(m)
1	234.06	228.88
2	232.17	237.53
3	226.45	229.35
4	231.17	233.70
5	235.98	231.72
6	232.17	225.65
7	218.84	229.15

Table 6.1: Results of motion estimation using side sonar images. The results are compared to estimated distance by DVL, which is treated as ground truth.

Chapter 7

Conclusion

The goal of the work presented in this thesis was to present an algorithm that can adapt the parameters of an AUV's motion model. The work was primarily focused on developing and comparing an adaptive motion model to a static motion model. The use of side sonar images as a feedback to the algorithm enabled the algorithm to learn on the fly. Expectation maximization was used to learn the parameters in an unsupervised manner. The second part of the thesis focussed on validating our dynamic landmark approach. This was done by estimating motion from side sonar images and comparing it to DVL. The results of the first section is illustrated in an experiment to produce pose estimates by integrating the motion and sensor models. The pose estimates of static and adaptive motion model are compared and the localization error is plotted. The estimated distances by the algorithm on real side sonar datasets are presented in the results of the second section.

Probabilistic robotics has been the way to approach robotics for a long time. The motion and sensor model are key ingredients to any algorithms for navigation, localization and map building. These models are treated as Gaussian distribution with static parameters. The questions that arises is how these models react to changes in the environment and robots. Higher level task such as navigation and path planning are dependant upon the accuracy of these model. To adapt to these changes we need to change our parameters to a model with time.

Overall the work illustrated that adapting motion model can be extremely advantageous in decreasing the localization error which in turn helps a robot in better navigation and path planning. The estimated parameters accuracy depends upon the sensor noise and can be low but the goal of the thesis was to decrease the localization error over time with changes in environment. The method doesn't require any pre learning phase and helps in getting rid of the manual labour associated with the calibration process. The algorithm doesn't require the AUV to loop back in its path

to learn the right parameters for the model. The algorithm as per now is limited to two dimensions and work needs to be done to get it working for six degrees of freedom. The work presented here is in a simulator and I feel there needs to be some extra work done in terms of testing and porting the algorithm. The algorithm to generate side sonar images presented by Andrew Vardy [36] online needs to be tested. The algorithm requires work so that it can be ported and performance can be tested for an on board processor of the AUV. Overall the work presented here shows the importance of having an adaptive motion model for better localization of robots.

Bibliography

[1] Timothy D Barfoot. Online visual motion estimation using fastslam with sift features. In *Intelligent Robots and Systems, 2005.(IROS 2005). 2005 IEEE/RSJ International Conference on*, pages 579–585. IEEE, 2005.

[2] Christopher M Bishop and Nasser M Nasrabadi. *Pattern recognition and machine learning*, volume 1. springer New York, 2006.

[3] Zhe Chen. Bayesian filtering: From Kalman filters to particle filters, and beyond. *Statistics*, 182(1):1–69, 2003.

[4] Ingemar J Cox and Gordon Thomas Wilfong. *Autonomous robot vehicles*, volume 447. Springer-Verlag New York, 1990.

[5] Arthur P Dempster, Nan M Laird, and Donald B Rubin. Maximum likelihood from incomplete data via the EM algorithm. *Journal of the Royal Statistical Society. Series B (Methodological)*, pages 1–38, 1977.

[6] Arnaud Doucet, Simon J Godsill, and Mike West. Monte Carlo filtering and smoothing with application to time-varying spectral estimation. In *Acoustics, Speech, and Signal Processing, 2000. ICASSP'00. Proceedings. 2000 IEEE International Conference on*, volume 2, pages II701—-II704. IEEE, 2000.

[7] Arnaud Doucet and Adam M Johansen. A tutorial on particle filtering and smoothing: Fifteen years later. *Handbook of Nonlinear Filtering*, 12:656–704, 2009.

[8] Austin I Eliazar, Parr Cs, and Duke Edu. Learning Probabilistic Motion Models for Mobile Robots. 2004.

[9] J W Fishers. Side Scan Sonar. \url{http://www.jwfishers.com/sss.htm}.

[10] Simon J Godsill, Arnaud Doucet, and Mike West. Monte Carlo Smoothing for Nonlinear Time Series. *Journal of the American Statistical Association*, 99(465):156–168, March 2004.

[11] Neil J Gordon, David J Salmond, and Adrian F M Smith. Novel approach to nonlinear/non-Gaussian Bayesian state estimation. In *IEE Proceedings F (Radar and Signal Processing)*, volume 140, pages 107–113. IET, 1993.

[12] G Grisettiyz, Cyrill Stachniss, and Wolfram Burgard. Improving grid-based slam with rao-blackwellized particle filters by adaptive proposals and selective resampling. In *Robotics and Automation, 2005. ICRA 2005. Proceedings of the 2005 IEEE International Conference on*, pages 2432–2437. IEEE, 2005.

[13] Oddvar Hallingstad and Kongsberg Maritime. Comparison of Mathematical Models for the HUGIN 4500 AUV Based on Experimental Data Commonsfor dervabiov menfotionetepenotations hed so-led hdodmnamice depries . ntheionseis are oces andimomets . os the. (7491):17–20, 2007.

[14] Ø yvind Hegrenæ s, Einar Berglund, and Oddvar Hallingstad. Model-Aided Inertial Navigation for Underwater Vehicles. 2008.

[15] Oyvind Hegrenaes, Einar Berglund, and Oddvar Hallingstad. Model-aided inertial navigation for underwater vehicles. In *Robotics and Automation, 2008. ICRA 2008. IEEE International Conference on*, pages 1069–1076. IEEE, 2008.

[16] Rudolph Emil Kalman and Others. A new approach to linear filtering and prediction problems. *Journal of basic Engineering*, 82(1):35–45, 1960.

[17] Peter King, Andrew Vardy, Peter Vandrish, and Benjamin Anstey. Real-time side scan image generation and registration framework for AUV route following. In *Autonomous Underwater Vehicles (AUV), 2012 IEEE/OES*, pages 1–6. IEEE, 2012.

[18] Andrew Lammas, Karl Sammut, and Fangpo He. 6-DoF Navigation Systems for Autonomous Underwater Vehicles. 2004.

[19] S M LaValle. *Planning Algorithms*. Cambridge University Press, Cambridge, U.K., 2006.

[20] John J Leonard, Andrew A Bennett, Christopher M Smith, and H Feder. Autonomous underwater vehicle navigation. In *IEEE ICRA Workshop on Navigation of Outdoor Autonomous Vehicles*, 1998.

[21] David G Lowe. Object recognition from local scale-invariant features. In *Computer vision, 1999. The proceedings of the seventh IEEE international conference on*, volume 2, pages 1150–1157. Ieee, 1999.

[22] Thomas Minka. Expectation-Maximization as lower bound maximization. *Tutorial published on the web at http://www-white. media. mit. edu/tpminka/papers/em. html*, 1998.

[23] Office of Coast Survey. Side Scan Sonar. \url{http://www.nauticalcharts.noaa.gov/hsd/SSS.html}.

[24] Branko Ristic, Sanjeev Arulampalm, and Neil James Gordon. *Beyond the Kalman filter: Particle filters for tracking applications*. Artech House Publishers, 2004.

[25] Marshall N Rosenbluth and Arianna W Rosenbluth. Monte Carlo calculation of the average extension of molecular chains. *The Journal of Chemical Physics*, 23:356, 1955.

[26] N. Roy and S. Thrun. Online self-calibration for mobile robots. *Proceedings 1999 IEEE International Conference on Robotics and Automation (Cat. No.99CH36288C)*, 3:2292–2297.

[27] Stuart Russell. *Artificial intelligence: A modern approach, 2/E*. Pearson Education India, 2003.

[28] Davide Scaramuzza and Roland Siegwart. Appearance-guided monocular omnidirectional visual odometry for outdoor ground vehicles. *Robotics, IEEE Transactions on*, 24(5):1015–1026, 2008.

[29] Stephen Se, David Lowe, and Jim Little. Vision-based mobile robot localization and mapping using scale-invariant features. In *Robotics and Automation, 2001. Proceedings 2001 ICRA. IEEE International Conference on*, volume 2, pages 2051–2058. IEEE, 2001.

[30] Jonathan Richard Shewchuk. An introduction to the conjugate gradient method without the agonizing pain, 1994.

[31] Silvia Silva, Paulo Drews Jr, Gabriel Leivas Oliveira, and Silva Figueiredo. Visual Odometry and Mapping for Underwater Autonomous Vehicles.

[32] Fossen Thor. Guidance and Control Of Ocean Vechiles.

[33] Sebastian Thrun, Wolfram Burgard, Dieter Fox, and Others. *Probabilistic robotics*, volume 1. MIT press Cambridge, MA, 2005.

[34] USGS. WHSC Sidescan Sonar Systems. \url{http://woodshole.er.usgs.gov/operations/sfmappi

[35] Utkarsh. SIFT: Scale Invariant Feature Transform. \url{http://aishack.in/2010/05/sift-scale-invariant-feature-transform/}, 2010.

[36] Peter Vandrish, Andrew Vardy, Dan Walker, and O A Dobre. Side-scan sonar image registration for AUV navigation. In *Underwater Technology (UT), 2011 IEEE Symposium on and 2011 Workshop on Scientific Use of Submarine Cables and Related Technologies (SSC)*, pages 1–7. IEEE, 2011.

[37] Miomir Vukobratovic. *Introduction to robotics*. Springer-Verlag Berlin, Germany, 1989.

[38] Teddy N. Yap and Christian R. Shelton. Simultaneous learning of motion and sensor model parameters for mobile robots. *2008 IEEE International Conference on Robotics and Automation*, pages 2091–2097, May 2008.